

## Spectral Emissivity Profiles for Radiative Cooling

Muhammed Ali Kecebas, Pinar Menguc, and Kursat Sendur\*

Cite This: <https://doi.org/10.1021/acsaom.3c00092>

Read Online

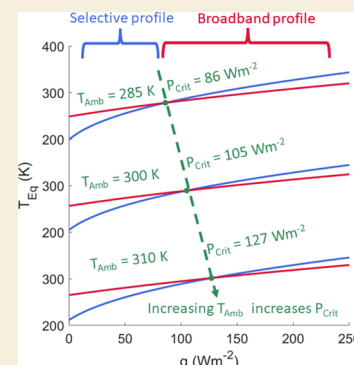
ACCESS |

Metrics &amp; More

Article Recommendations

**ABSTRACT:** Passive radiative cooling, an innovative approach for cooling buildings and devices, has attracted considerable attention in recent years. In particular, the spectral emissivity distribution of surfaces plays a crucial role for an object to radiate at wavelengths for which the atmosphere is transparent and solar irradiance is low. Here, we study the role of spectral emissivity distributions using different performance metrics: cooling power (CP) and equilibrium temperature ( $T_{\text{Eq}}$ ). We investigated the roles of environmental factors, such as ambient temperature and level of thermal insulation from surroundings, on spectral emissivity distributions. Based on these emissivity distributions, we report the conditions at which the suitable profile for cooling power maximization and equilibrium temperature minimization changes. We discuss the realization of spectral emissivity distributions using various optical materials for cooling power maximization and equilibrium temperature minimization separately under different environmental conditions. The impacts of material selection on the realization of desired emissivity profiles and corresponding outcomes are analyzed. As progress in this emerging field gains traction, development of radiative cooling structures with suitable spectral emissivity profiles under different circumstances will become essential.

**KEYWORDS:** Radiative cooling, radiative heat transfer, emissivity, thermal insulation, cooling power, equilibrium temperature



## 1. INTRODUCTION

Passive radiative cooling, a heat exchange mechanism which occurs between terrestrial objects and the outer sky via the atmospheric transmission window, has attracted significant interest as the demand for energy efficient cooling solutions increases. Although the concept of radiative cooling below ambient air temperature was initially demonstrated in the mid 1970s<sup>1</sup> for nighttime conditions, its demonstration under direct sunlight in 2014<sup>2</sup> reignited the interest of researchers. It was shown that selective engineering of the spectral properties of the surface is a core requirement for radiative cooling during both nighttime and daytime. The fundamental mechanism that allows radiative cooling, independently from operation time, is the simultaneous emission of thermal radiation in the 8–13  $\mu\text{m}$  range at which surfaces with temperatures around 300 K radiate<sup>3</sup> and suppression of absorption at shorter and longer wavelengths prevent absorption of atmospheric thermal radiation.<sup>4</sup> Even though the suppression of absorption in the 4–8  $\mu\text{m}$  range and wavelengths longer than 13  $\mu\text{m}$  are sufficient to prevent a significant portion of the radiation from the atmospheric contributions, absorption at wavelengths shorter than 4  $\mu\text{m}$  must be strongly suppressed to avoid the absorption of solar irradiance, which is present during the daytime. Based on these requirements, a selective profile is proposed and realized with a multilayer structure and shown to be effective in achieving steady state temperature below ambient under direct sunlight.<sup>2</sup> In the following years, many different types of structures have been proposed in the

literature.<sup>5–11</sup> In addition to these fundamental studies on various types of structures, the integrations of radiative cooling structures with photovoltaics<sup>12–14</sup> and buildings<sup>15–21</sup> were reported. Because of the thermal insulation requirement of radiative cooling, progress in development of thermal covers has been a research field of interest.<sup>22–24</sup> Considering the variations in demand during seasonal transitions, structures with dynamical radiative cooling capabilities were explored.<sup>25–31</sup> Challenges toward the commercialization of radiative cooling were also discussed in the literature.<sup>32,33</sup>

After successful demonstrations of radiative cooling with a variety of structures, a few studies are focused on the role of emissivity profiles on the performance of radiative cooling.<sup>9,34,35</sup> Especially in ref 35, different types of emissivity profiles are discussed in detail which leads to lower equilibrium temperatures under different conditions. In the light of these discussions regarding the emissivity profiles, existing literature should be reassessed in detail with the consideration of the applicability of the proposed structures in achieving the altered emissivity profiles. Radiative cooling performances of different emissivity profiles have been demonstrated experimentally,

**Special Issue:** Optical Materials for Radiative Cooling

**Received:** March 10, 2023

**Revised:** May 29, 2023

**Accepted:** May 30, 2023

which provides an idea about the limits that can be achieved through radiative cooling. In ref 36, steady state temperature lower than ambient by 40 °C is achieved with a structure that only has a strong emission in the 8–13  $\mu\text{m}$  range. Later, it is shown that using a narrowband emission profile instead of selectively emitting in the 8–13  $\mu\text{m}$  range can lead to temperature reductions of 100 °C below ambient temperature.<sup>35,37</sup> However, it is shown that achieving such extreme low temperatures requires near-complete thermal isolation of nonradiative heat exchange mechanisms. Considering the challenge in achieving such high isolation, necessary modifications to emissivity profiles are analyzed in refs 9 and 35, and the need for broadening the emission spectrum is demonstrated. In addition to temperature reduction, the possible differences in emissivity profiles are also reported when the cooling power of the surface is of interest.

Many different materials and system architectures can be used to realize these emissivity profiles. These material systems are enabled by advancements in computational design, fabrication, and characterization tools of optical structures.<sup>38–51</sup> Multilayers, micro/nanoparticle-embedded polymeric coatings, and polymers with artificially engineered porosities are among some of the structures that are utilized for radiative cooling purposes. Layered structures which consist of a combination of different materials are one of the simplest, yet very effective, ways of realizing the desired emissivity profile for radiative cooling.<sup>2,52–58</sup> Usually, materials with strong absorption in the 8–13  $\mu\text{m}$  wavelength range and near-lossless in the visible and near-infrared spectra, such as  $\text{SiO}_2$ ,  $\text{Al}_2\text{O}_3$ ,  $\text{TiO}_2$ ,  $\text{HfO}_2$ ,<sup>59</sup> are used together with a metal which provides broadband reflection. Tailoring of the interference of the propagating wave components inside the structure is the fundamental mechanism that leads to target spectral characteristics. Although many of the proposed multilayer structures are composed of periodically alternating layers of high–low index materials,<sup>2,52,53,60,61</sup> various numerical methods optimize the layer thicknesses together with the selected materials from a predefined material library.<sup>53,62,63</sup> However, while designing multilayers, especially with a combination of different materials, possible fabrication challenges and the feasibility of extension to large scale should be considered. A simple structure proposed in the literature addresses such challenges,<sup>64</sup> which is composed of a single PDMS layer on top of Ag. Such a simple structure is shown to be effective in achieving radiative cooling below ambient temperature, which exhibits an 8 °C lower surface temperature than ambient temperature, with 127  $\text{Wm}^{-2}$  cooling power at ambient temperature.

As an alternative to the aforementioned stacked layers, it is shown that radiative cooling performance of single layered coatings can be further improved by embedding micro/nanoparticles.<sup>65–73</sup> The first experimental demonstration of such a structure is reported in 2017,<sup>73</sup> for which a cooling power of nearly 95  $\text{Wm}^{-2}$  is reported. The major advantage of this type of structure over layered structures is its feasibility for large scale production. Following the successful demonstration of a particle-based structure on passive radiative cooling in the daytime, different configurations of micro/nanoparticle-based polymeric structures composed of mixtures of different materials have been reported in recent years. Although most of these structures are suitable for large scale fabrication, they still require a metallic back reflector to satisfy increases in the

fabrication steps, thus hindering the feasibility of extension to large scale.

Metamaterials consisting of periodically arranged surface textures are among other widely used methods to achieve radiative cooling.<sup>74</sup> Due to their capability of exciting different resonance mechanisms, e.g., lattice and plasmonic resonances,<sup>75–81</sup> they are excellent candidates for satisfying the strong emission in the 8–13  $\mu\text{m}$  wavelength interval. In fact, the first theoretical demonstration of daytime passive radiative cooling is done by a multilayer structure combined with a periodically arranged surface texture.<sup>82</sup> A two-dimensional periodic array of square air holes composed of  $\text{SiC}$  and  $\text{SiO}_2$  are used to excite phonon–polariton resonances of these materials in the 8–13  $\mu\text{m}$  interval. The resulting emission spectrum provides near-perfect emission in the 8–13  $\mu\text{m}$  range, as well as the other possible atmospheric transparency window located in the 15–25  $\mu\text{m}$  interval. The major drawback of this structure despite its excellent spectral selectivity is the strong absorption in the visible spectrum due to  $\text{SiC}$ , which increases the heat load in the system. Following this idea, structures that utilize various types of grating like patterns are proposed<sup>83–88</sup> which allow controlling the wave–matter interaction at smaller geometries. It is also shown that broadband absorption achieved by stacking individual resonators in a trapezoidal fashion<sup>89</sup> can be utilized for radiative cooling purposes by designing a broadband selective absorber.<sup>90</sup> In addition, 2D metamaterials are widely used as radiative cooling structures to be integrated with devices that demand cooling, e.g., solar cells.<sup>91–95</sup> Because of their excellent spectral selectivity, metamaterials comply well with the devices' spectral requirements as well as the radiative cooling requirements. The same characteristic of metamaterials allows tailoring spectral characteristics for addressing other practical requirements such as colorization for aesthetic purposes. Recently, there has been increased attention to colored radiative cooling coatings<sup>96–108</sup> for which many types of metamaterials are proposed as great solutions thanks to their capability of selective spectral engineering.

A recently proposed type of polymeric structure at which porosity of the polymer was artificially engineered was shown to be effective in achieving solar irradiance reflection and emission in the atmospheric transparency window simultaneously.<sup>109–116</sup> While holes inside the structure act as a cavity at longer wavelengths, they exhibit a large bandgap and lead to broadband reflection in visible and near-infrared spectra at which solar irradiance is strong. Eliminating the need for an additional metallic layer is a major step toward large scale fabrication feasibility, thus allowing practical realization of passive radiative cooling coatings with readily available approaches and formats, such as paints.<sup>117</sup>

Parallel to research related to structural characteristics, there is also ongoing active research regarding the possible materials for use in radiative cooling coatings.<sup>6,10,17,118,119</sup> In ref 118, different candidate materials are reported not only for their spectral characteristics but also for their thermomechanical characteristics. Progress in this aspect of the field is equally important in terms of the development of radiative coolers with superior performances and characteristics for specific applications, e.g., buildings and solar cells. A recent example for a material aspect in the field is related to the use of plasmonics for colorization of a radiative cooling structure.<sup>120</sup>

There are extensive efforts to adapt the materials and structures that already exist in biological creatures or in the nature.<sup>121–124</sup> In 2015, right after the first experimental

demonstration of daytime passive radiative cooling in 2014,<sup>2</sup> it was shown that Saharan silver ants already benefit from daytime passive radiative cooling.<sup>125</sup> With the dense array of triangular hairs on their body, they are able to strongly reflect incident solar irradiance while emitting thermal radiation in the infrared spectrum simultaneously. A major advantage of such discoveries is that they provide excellent guidelines for future studies in the field. For instance, following ref 125, many artificially engineered structures that are inspired by Saharan ants were reported.<sup>126–129</sup> Another advantage of such bioinspired structures is that they provide candidate materials that are feasible for large fabrication and low cost and are ecofriendly. For instance, it was shown that through delignification and densification of natural wood, a mechanically strong highly efficient radiative cooling structure can be obtained.<sup>130</sup> Cellulose nanofibers are held responsible from high backscattering of solar irradiance and emission in mid-infrared wavelengths. After the demonstration of the potential of cellulose as a material for radiative cooling, many other works that propose cellulose-based radiative coolers were demonstrated.<sup>131–136</sup> Many other types of bioinspired structures and materials were also reported up to this date,<sup>137–145</sup> including studies based on near-field radiative transfer.<sup>146,147</sup> Finally, the radiative cooling capability of natural silk<sup>148</sup> opens the way for realizing radiative cooling phenomenon in textiles.<sup>149–158</sup> Successful demonstrations of radiative cooling with textiles considerably enlarges the application area and its potential contribution to energy consumption in general.

Despite the vast progress made in the field regarding the implementation of radiative cooling structures, the connection between the spectral characteristics of the coatings and radiative cooling dynamics is not explored in detail. More explicitly, the impact of spectral characteristics from the visible to far-infrared portions of the electromagnetic spectrum on the radiative characteristics, such as cooling power,  $P_{Cool}$  and equilibrium temperature,  $T_{Eq}$ , should be well considered. In addition, dependency of spectral requirements both for  $P_{Cool}$  maximization and  $T_{Eq}$  minimization, under various circumstances (ambient temperature and level of thermal insulation from the environment) must be well defined,<sup>35</sup> to develop radiative cooling structures that are more suitable to practical needs. Once the impact of environmental conditions on the spectral profiles are defined, estimates of theoretical limits can be created, and how close we can approach those limits can be observed.

In this work, starting with the fundamentals of radiative cooling and definition of its performance metrics,  $P_{Cool}$  and  $T_{Eq}$ , we studied the role of spectral emissivity of a surface on those under different conditions. Then, we designed 1D photonic multilayers specifically to maximize  $P_{Cool}$  and minimize  $T_{Eq}$  similar to the method described in ref 53 as a measure of how much we can approach the theoretically estimated limits. Structures are designed with different materials to discuss the role of optical properties on achieving desired spectra for  $P_{Cool}$  maximization and  $T_{Eq}$  minimization. Finally, we conclude with a brief summary.

## 2. FUNDAMENTALS OF RADIATIVE COOLING

Radiative cooling is a passive phenomenon that benefits from the tremendous temperature difference between the sky, 3 K, and terrestrial objects. Due to this temperature difference, a considerable heat exchange occurs between the sky and

terrestrial objects. To properly analyze a radiative cooling system, other radiative heat exchange mechanisms, such as solar irradiance and atmospheric thermal radiation, should also be taken into account. Earth receives a high amount of thermal radiation from the Sun, reaching up to  $1000 \text{ Wm}^{-2}$  levels at certain locations. A significant portion of the incident solar radiation is confined in visible and near-infrared spectra. In addition to solar irradiance, gas molecules in the Earth's atmosphere also emit thermal radiation. Therefore, together with the spectral characteristics of the radiation from terrestrial objects, characteristics of incoming radiation from various sources should be considered.

With the knowledge of the characteristics of these radiation mechanisms, their behaviors can be modeled and used to define the net heat exchange occurring on the surface, which determines the cooling power of the surface. In a similar manner, the temperature of the surface at equilibrium or steady state temperature can be estimated. These two are the most commonly used metrics to compare the performances of different radiative cooling systems. Therefore, the definition of cooling power and equilibrium temperature, as well as understanding of the parameters they are dependent on, are crucial for development of radiative cooling structures.

### 2.1. Cooling Power and Equilibrium Temperature

Cooling power of a surface is defined as the required energy exchange rate, in the form of heating or heat removal, to keep the temperature of the surface constant.<sup>159</sup> The net cooling power,  $P_{Cool}$  of a surface is mathematically defined in terms of ingoing and outgoing energy components that cause a change in the temperature of the surface

$$P_{Cool}(T_s) = P_{Rad}(T_s, \epsilon_s) - P_{Atm}(T_{Amb}, \epsilon_s, \epsilon_{Atm}) - P_{Sun}(\epsilon_s) \quad (1)$$

where  $P_{Rad}$  is the radiation from the surface,  $P_{Atm}$  is the absorbed atmospheric thermal radiation, and  $P_{Sun}$  is the absorbed solar irradiance. Nonradiative contributions can be included in eq 1 by adding  $P_{Conv} = h_c(T_s - T_{Amb})$  and  $q_i$ , where  $P_{Conv}$  is the heat flux due to convective heat transfer between the surface and ambient temperature, and  $q_i$  is the heat generated by the system during its operation. With these additional contributions, the net cooling power of a surface is defined as

$$P_{Cool}(T_s) = P_{Rad}(T_s, \epsilon_s) - P_{Atm}(T_{Amb}, \epsilon_s, \epsilon_{Atm}) - P_{Sun}(\epsilon_s) + P_{Conv} - q_i \quad (2)$$

From eq 2, for  $P_{Cool}$  maximization at any  $T_s$ , outgoing heat flux,  $P_{Rad}$  must be maximized while total incoming flux,  $P_{Atm}$ ,  $P_{Sun}$ ,  $P_{Conv}$  and  $q_i$  must be minimized through engineering of  $\epsilon_s$ .

Equilibrium temperature,  $T_{Eq}$ , on the other hand, is defined as the temperature at which heat exchange between the surface and its environment no longer occurs. This condition is mathematically expressed as

$$P_{Cool}(T_{Eq}) = 0 \Rightarrow P_{Rad}(T_{Eq}, \epsilon_s) = P_{Atm}(T_{Amb}, \epsilon_s, \epsilon_{Atm}) + P_{Sun}(\epsilon_s) - P_{Conv} + q_i \quad (3)$$

As seen, the condition given in eq 3, the condition for  $T_{Eq}$  minimization is significantly different than the  $P_{Cool}$  maximization. In the case of  $T_{Eq}$  minimization, incoming heat flux should be minimized such that it is compensated by outgoing

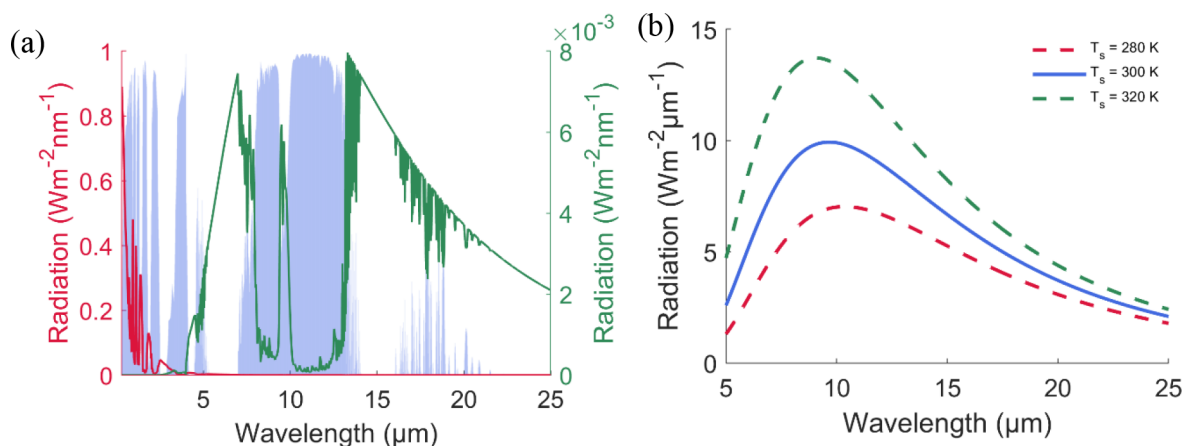


**Figure 1.** (a) Solar irradiance (red), transmission of the atmosphere (blue), and atmospheric thermal radiation at  $T_{Amb} = 300$  K (green). (b) Blackbody radiation from a surface at increasing temperatures,  $T_s = 280, 300$  and  $320$  K at  $5\text{--}25$   $\mu\text{m}$  spectrum interval.

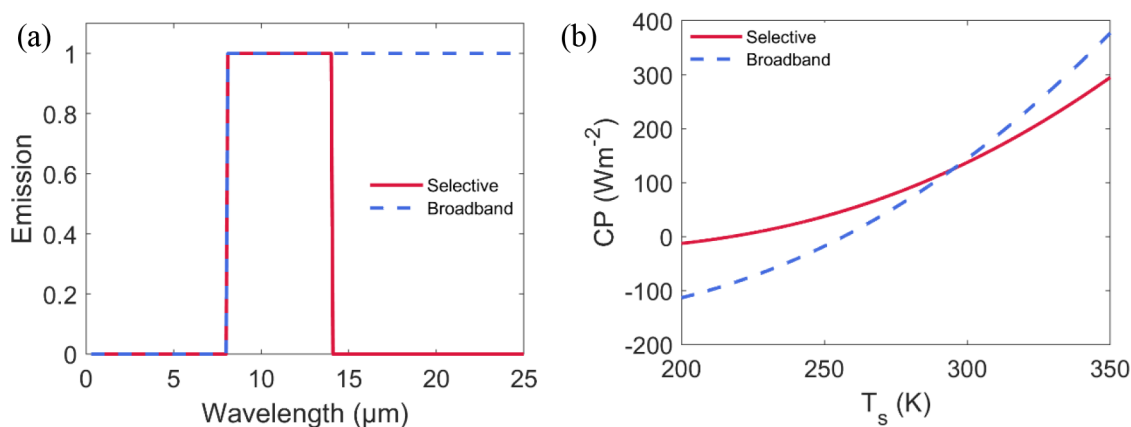


**Figure 2.** (a) Selective emission,  $\varepsilon(\lambda) = 1$  when  $8 < \lambda < 13$   $\mu\text{m}$  and  $\varepsilon(\lambda) = 0$  elsewhere, and broadband emission,  $\varepsilon(\lambda) = 1$  when  $\lambda > 8$   $\mu\text{m}$  and  $\varepsilon(\lambda) = 0$   $\lambda < 8$   $\mu\text{m}$  profiles. (b) Corresponding  $T_s\text{--}P_{Cool}(T_s)$  curves for the selective and broadband emission profiles.

flux, the radiation from a surface at temperature  $T_{Eq}$ . In other words, maximum  $P_{Cool}$  is achieved when the difference between incoming and outgoing heat fluxes are maximized, whereas  $T_{Eq}$  is minimized when incoming heat flux is minimum.

As seen, both  $P_{Cool}$  and  $T_{Eq}$  are strongly dependent on the radiation characteristics from the surface that is cooling of interest, as well as the heating inputs that are acting on the surface. Therefore, it is crucial to understand the characteristics of both radiative and nonradiative components to maximize and minimize the  $P_{Cool}$  and  $T_{Eq}$ .

## 2.2. Understanding the Dynamics of Radiative Components and their Role in CP and $T_{Eq}$

As discussed in the previous section, when a surface is exposed to the sky, contributions from atmospheric thermal radiation and solar irradiance should be considered during the heat exchange analysis. In general, both solar irradiance and atmospheric thermal radiation are dependent on geographical conditions as well as the time of the year. Mathematical expressions for the atmospheric thermal radiation and solar irradiance are available and extensively used in the analysis of radiative cooling, which are given as

$$P_{Atm}(T_{Amb}, \varepsilon_s, \varepsilon_{Atm}) = A \int d\Omega \cos \theta \int_0^\infty d\lambda I_{BB}(T_{Amb}, \lambda) \varepsilon_{Atm}(\lambda, \theta) \varepsilon_s(\lambda, \theta) \quad (4)$$

$$P_{Sun}(\varepsilon_s) = A \int_0^\infty d\lambda I_{AM}(\lambda) \varepsilon_s(\lambda, \theta) \quad (5)$$

where  $\int d\Omega = 2\pi \int_0^{\pi/2} d\theta \sin \theta$ .  $T_{Amb}$  and  $\varepsilon_{Atm}$  stand for ambient air temperature and emissivity of the atmosphere, respectively, which are modeled as  $1 - (t_{Atm})^{1/\cos \theta}$  where  $t_{Atm}$  is the transmissivity of the atmosphere. As seen from eqs 4 and 5,  $P_{Atm}$  is modeled as radiation from a diffusive surface at ambient temperature whereas solar irradiance is assumed to be direct and therefore has no angular integral. For both cases, it is assumed that  $\varepsilon_s(\lambda, \theta)$  is equal to angular and spectral absorption,  $\alpha_s(\lambda, \theta)$ , of the surface according to Kirchhoff's law of thermal radiation. In Figure 1(a), typical solar irradiance and atmospheric thermal radiation when  $T_{Amb} = 300$  K are shown together with the  $t_{Atm}$ . As seen, solar irradiance is highly confined in the visible spectrum,  $0.3\text{--}0.7$   $\mu\text{m}$  interval, and significantly lower at longer wavelengths. On the other hand, atmospheric thermal radiation takes place at longer wavelengths, from  $5$  to  $25$   $\mu\text{m}$  with a low radiation region in the  $8\text{--}13$   $\mu\text{m}$  range, which is referred to as atmospheric transparency window. These two components are usually considered as fundamental radiative heat loads acting on the surface when exposed to the sky. Spectral distribution of these sources determines the spectral emissivity requirement for radiative cooling, together with the emitted radiation from the surface,  $P_{Rad}$  for which the mathematical expression is given as

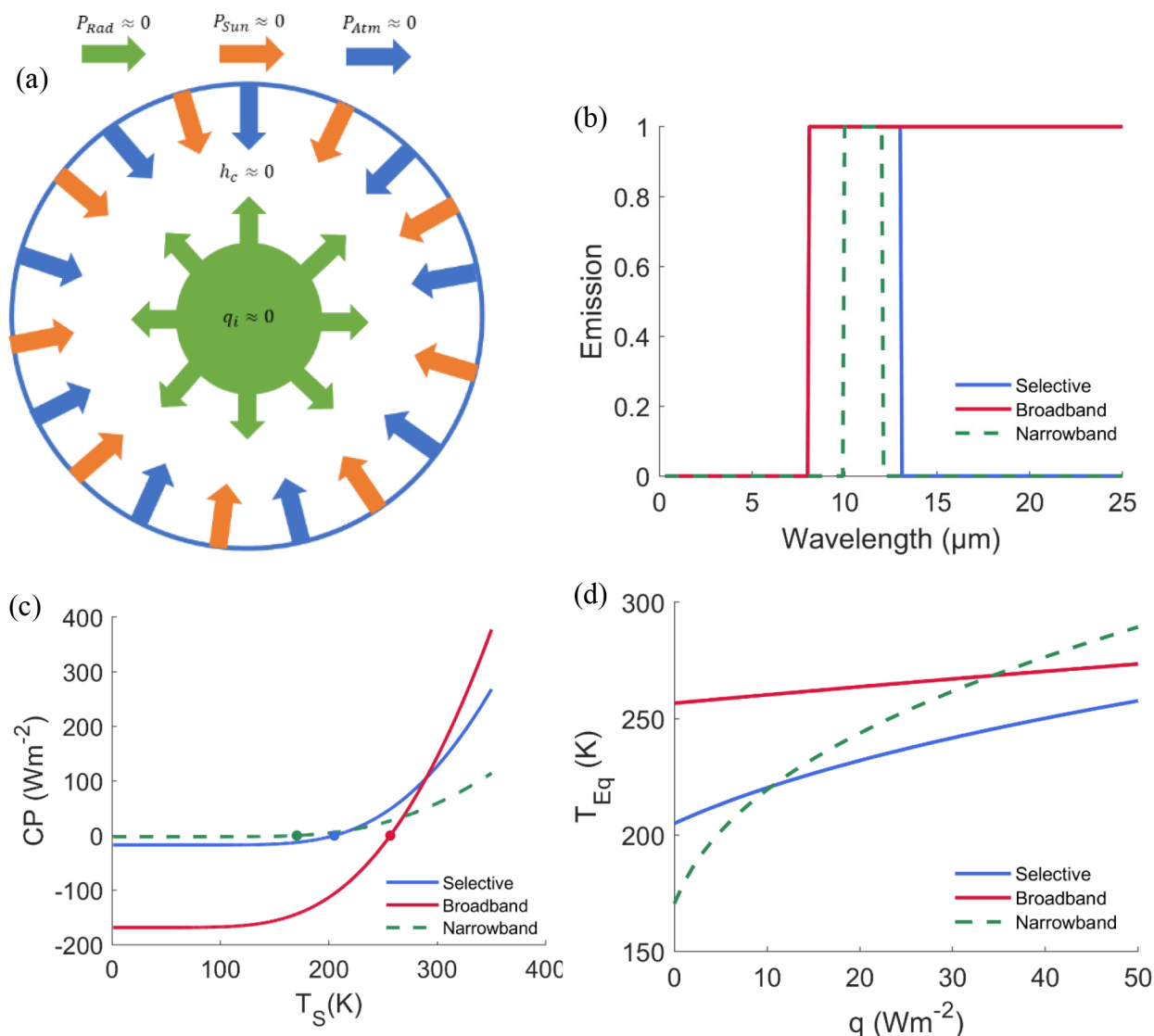


**Figure 3.** (a) Schematic representation of a thermally closed system. (b) Comparison of selective, broadband, and narrowband emissivity profiles. (c) Corresponding  $T_s$ - $P_{Cool}$  profiles for selective, broadband, and narrowband emissivity profiles with  $T_{Eq}$  points marked. (d) Change of  $T_{Eq}$  with increasing  $q$  for selective, broadband, and narrowband emissivity profiles.

$$P_{Rad}(T_s, \epsilon_s) = A \int d\Omega \cos \theta \int_0^\infty d\lambda I_{BB}(T_s, \lambda) \epsilon_s(\lambda, \theta) \quad (6)$$

The sources of the difference between  $P_{Rad}$  and  $P_{Atm}$  are as follows: The difference between the radiation temperatures,  $T_s$  and  $T_{Amb}$ , and the contribution of  $\epsilon_{Atm}(\lambda, \theta)$  only affects  $P_{Atm}$ . Since  $\epsilon_{Atm}(\lambda, \theta)$  is always lower than 1,  $P_{Atm}$  will always be lower than  $P_{Rad}$  when  $T_s \geq T_{Amb}$ , because of the spectral distributions of  $I_{BB}(T_{s, \lambda})$  and  $I_{BB}(T_{Amb, \lambda})$  as depicted in Figure 1(b).

Based on these characteristics of  $P_{Rad}$ ,  $P_{Atm}$ , and  $P_{Sun}$  have spectral requirements for the purpose of  $P_{Cool}$  maximization and  $T_{Eq}$  minimization through passive radiative cooling. It is important to note that nonradiative dynamics should also be considered during the derivation of the spectral requirements, since they have significant effects on the total heat load acting on the surface.

### 3. SPECTRAL REQUIREMENTS OF RADIATIVE COOLING

In this section, we analyze the resulting  $P_{Cool}$  and  $T_{Eq}$  differences of the two different emissivity profiles, which are referred to as selective and broadband emission profiles, as shown in Figure 2(a). The selective profile depicted in Figure 2(a) is considered as the *ideal* profile for radiative cooling below ambient air temperature. The other profile, which has unity emission after  $8 \mu\text{m}$ , is considered in the literature for cooling of the systems with relatively higher temperatures. As a reference point, we started analysis of these profiles by setting  $h_c = q_i = 0$ . With this condition, the surface's cooling power and  $T_{Eq}$  are calculated under the assumption of an isolated system from the nonradiative heat exchange. In such a case,  $T_{Eq}$  values for those profiles are 204 and 256 K, and they exhibit different  $P_{Cool}$  values, especially at higher temperatures than  $T_{Amb}$ . In terms of  $T_{Eq}$  reduction, a selective profile yields significantly better performance than the broadband profile when the system is isolated. However, it is not a very realistic scenario considering the challenges in achieving such an extreme

thermal isolation. In fact, radiative coolers are designed to be integrated to the systems that heat up during their operation and require cooling. Therefore, generated heat from the system must be transferred to the radiative cooler and emitted away, which leads to  $q_i \neq 0$ . Such a condition may cause changes in the required spectral profiles, e.g., transition to selective to broadband, as in ref 93. Therefore, it is important to understand how spectral requirements vary with respect to external factors for understanding the limits of the radiative cooling.

To analyze the changes in spectral requirements, especially to find the transition point from the selective to broadband profile, outcomes of those profiles are analyzed under different conditions. For analysis purposes, we introduce the term  $P_L$ , which stands for the total heat load acting on the surface, e.g., all heat contributions coming from absorption of solar irradiance and atmospheric thermal radiation, as well as nonradiative contributions, and it can be mathematically expressed as  $P_L = P_{Atm}(T_{Amb}, \epsilon_s, \epsilon_{Atm}) + P_{Sun}(\epsilon_s) + q_i + P_{Conv}$ .

### 3.1. $P_{Cool}$ Maximization

Cooling power is maximized when the difference between  $P_{Rad}$  and  $P_L$  is maximum. Here, it is important to note that when  $T_s > T_{Amb}$ ,  $P_{Conv}$  will contribute positively to  $P_{Cool}$ , whereas it will be the opposite when  $T_s < T_{Amb}$ . In addition, it is already shown that when  $T_s \geq T_{Amb}$ ,  $P_{Rad}$  will always be higher than  $P_{Atm}$  leading to higher  $P_{Cool}$ . Based on these, the following two cases are analyzed for selective and broadband profiles.

**3.1.1.  $T_s < T_{Amb}$ .** When  $T_s < T_{Amb}$ , unlike the opposite scenario,  $P_{Rad}$  is not unconditionally higher than  $P_{Atm}$  but will be highly dependent on spectral distributions of  $\epsilon_s$  and  $\epsilon_{Atm}$ . In such a case,  $\epsilon_s$  should be engineered such that it is minimum at the wavelengths at which atmospheric thermal radiation,  $I_{BB}(T_{Amb}, \lambda) \epsilon_{Atm}(\lambda, \theta)$ , is high so that the surface does not absorb more power than it emits. From these, it appears that achieving a positive  $P_{Cool}$  requires more strict spectral requirements when  $T_s < T_{Amb}$ . As seen, for the selective profile,  $\epsilon_s$  is zero when  $\epsilon_{Atm}(\lambda, \theta)$  is high,  $T_{Atm}(\lambda, \theta)$  is low, and it is maximum elsewhere. If the surface had strong emission at  $\lambda > 13 \mu\text{m}$ , it would absorb more power coming from atmospheric thermal radiation. In addition, since  $T_s < T_{Amb}$ , emitted radiation at  $\lambda > 13 \mu\text{m}$  would be lower than absorbed atmospheric thermal radiation. Therefore, the surface does not benefit from emitting radiation at  $\lambda > 13 \mu\text{m}$  at all, which makes selective emission profile superior compared to the broadband profile in terms of  $P_{Cool}$  maximization. It is also apparent when the  $T_s - P_{Cool}$  curve depicted in Figure 2(b) is considered. As seen, when  $T_s < T_{Amb}$  the selective emission profile exhibits higher  $P_{Cool}$ .

**3.1.2.  $T_s \geq T_{Amb}$ .** When  $T_s \geq T_{Amb}$ ,  $P_{Rad}$  will always be higher than  $P_{Atm}$  because of the characteristics of thermal radiation from surfaces. Considering the radiation at  $\lambda > 13 \mu\text{m}$ ,  $P_{Rad}$  can benefit from radiation at those wavelengths, despite the characteristics of atmospheric transparency. Therefore, when the  $T_s - P_{Cool}$  curve for the broadband profile is considered,  $P_{Cool}$  is higher for the broadband profile at temperatures higher than ambient temperature, compared to the selective emission profile. This reasoning is valid any  $T_{Amb}$ ,  $h_c$ , and  $q_i$  because those characteristics do not alter the radiation characteristics that are considered for this conclusion. Therefore,  $P_{Cool}$  maximization surfaces can benefit from radiation at  $\lambda > 13 \mu\text{m}$ , if the surface temperature is above the ambient temperature.

### 3.2. $T_{Eq}$ Minimization

Although the  $P_{Cool}$  enhancement problem can be mathematically considered as maximization of a difference,  $\max(P_{Rad} - P_L)$ , it is not the case for  $T_{Eq}$  minimization. In fact,  $T_{Eq}$  minimization should be treated as a minimization problem,  $\min(P_L)$ , so that it can be compensated by  $P_{Rad}(T_{Eq})$ . Physically speaking,  $T_{Eq}$  is the temperature at which radiation from the surface (only outgoing radiative channel for heat exchange, if  $T_s$  is below ambient) compensates all heat load present in the system. Therefore, emission can be treated as the radiative heat load if the system is strictly minimized. This is in contrast to the case for  $P_{Cool}$  maximization.

In the case of a near-complete isolation of the system as depicted in Figure 3(a),  $h_c \approx q_i \approx 0$ , and with complete reflection in the entire electromagnetic spectrum,  $T_{Eq}$  can be reduced to extremely low values. In such a case,  $P_L$  will be very low, considering  $P_{Atm} \approx P_{Sun} \approx 0$  due to near-complete reflection; therefore, even a very small amount of thermal radiation from the surface can compensate for  $P_L$ . To analyze such a scenario, a new emissivity profile, referred as the *narrowband*, is created as seen in Figure 3(b). As opposed to the selective emissivity profile, emission occurs in a narrower wavelength interval, 10–12  $\mu\text{m}$ . When  $h_c \approx q_i \approx 0$ , only heat load in the system will be due to  $P_{Atm}$ , which is 1.9  $\text{W}/\text{m}^2$ . It means that the temperature,  $T_s$ , that satisfies the following,

$$P_{Rad}(T_s, \epsilon_{\text{Narrowband}}) \quad \text{will be } T_{Eq} \quad \text{When } T_s - P_{Cool} = P_{Atm}(T_s, \epsilon_{\text{Narrowband}}, \epsilon_{Atm}) = 1.9 \text{ Wm}^{-2}$$

curves are constructed for these three profiles,  $T_{Eq}$  for the narrowband profile is obtained as 170 K which is nearly 35 K lower than that of the selective profile.  $T_{Eq}$  for the broadband profile is 256 K, which is significantly higher than both. Since  $h_c \approx q_i \approx 0$ , reflection is set to unity until 8  $\mu\text{m}$  for each case; therefore,  $P_{Sun}$  is almost equal for each. The only difference between heat loads acting on the surfaces stems from  $P_{Atm}$  values which are 1.9, 16.2, and 167  $\text{Wm}^{-2}$ . When  $P_{Atm} = 1.9 \text{ Wm}^{-2}$ , radiation at 170 K is sufficient to compensate. On the other hand, as  $P_{Atm}$  increases, the heat load acting on the system can be compensated only with radiation at higher temperatures, leading to higher  $T_{Eq}$ . This example demonstrates the impact of heat load on the  $T_{Eq}$ .

To analyze the performance of the narrowband profile when  $P_L \gg 0$ ,  $q$  is increased gradually to simulate a heat load increase on the surface, and corresponding  $T_{Eq}$  values are calculated. As seen in Figure 3(d), when  $q$  is above 10  $\text{Wm}^{-2}$ ,  $T_{Eq}$  for the narrowband profile becomes higher than that of the selective profile. This indicates that, in the presence of a slight deviation from the complete reflection requirement in the visible and near-infrared spectra, the narrowband profile will lose its advantage over the selective profile. When such a strict requirement is considered together with the difficulty of realizing such a profile, utilizing the narrowband profile to cool the system purely with radiative cooling becomes infeasible.

When near-complete isolation is not the case, the  $P_L \gg 0$ , surface should emit more thermal radiation to compensate for the thermal load acting on the system; therefore, the selective profile becomes more suitable compared to the narrowband profile. Similar to the threshold for switching from the narrowband to the selective profile, a critical heat load,  $P_{Crit}$  can be defined to estimate the transition point from the selective to broadband emission profiles. In Figure 4,  $T_{Eq}$

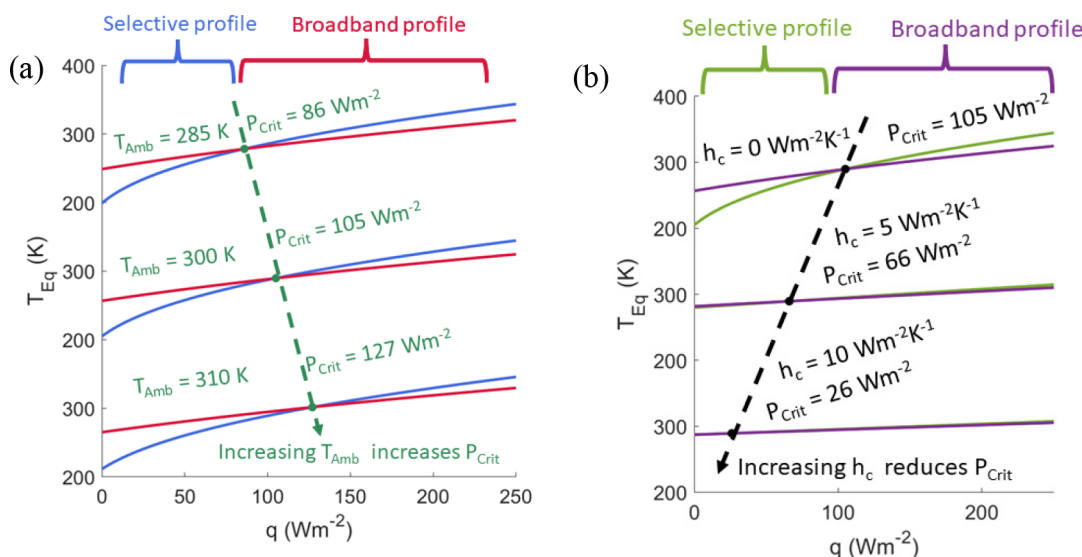


**Figure 4.**  $T_{Eq}$  with respect to increasing  $q$ : (a) at fixed  $h_c = 0$  and increasing  $T_{Amb}$  with transition points  $P_{Crit}$  (green) from selective profile (blue) to broadband profile (red) and (b) at fixed  $T_{Amb} = 297$  K and increasing  $h_c$  with transition points  $P_{Crit}$  (black) from selective profile (green) to broadband profile (purple).

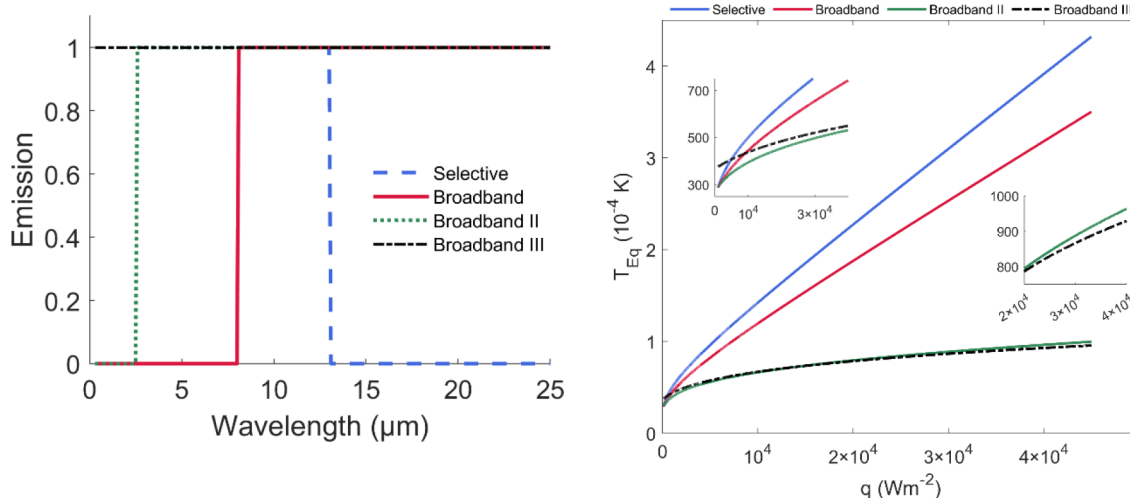


**Figure 5.** Comparison of selective and different broadband profiles with varying unity emission starting points. (b) Change of  $T_{Eq}$  with increasing  $q$  for selective and different broadband profiles.

values for increasing  $q_i$  are plotted for selective and broadband emission profiles for different  $T_{Amb}$  and  $h_c$  values. The transition from the narrowband to broadband occurs when  $q_i = 86 \text{ Wm}^{-2}$  at  $T_{Amb} = 285 \text{ K}$ , and when  $T_{Amb}$  is increased to  $310 \text{ K}$ , transition occurs when  $q_i = 127 \text{ Wm}^{-2}$ . The transition between the profiles occurs when the surface with the selective profile is not capable of compensating for the total heat load at a temperature lower than it would with a broadband profile. However, in the case of emission at  $\lambda > 13 \mu\text{m}$ , which leads to higher  $P_{Rad}$ ,  $P_{Atm}$  is also increased due to absorption of atmospheric thermal radiation at those wavelengths, which increases the total heat load acting on the system. Therefore, for the transition between profiles to occur, the rise in  $P_{Rad}$  should be greater than the increase in  $P_{Atm}$ . It is already known that higher  $T_{Amb}$  leads to higher  $P_{Atm}$ . When  $T_{Amb}$  is higher, the surface should emit more radiation to address for the increased  $P_{Atm}$  which is only possible at higher temperatures for a fixed emissivity. Because of this, the transition occurs at larger  $q_i$  for higher  $T_{Amb}$ , which causes higher surface temperatures. This

analysis reveals that the selective emission profile at higher  $T_{Amb}$  is superior compared to the broadband profile up to higher heat loads.

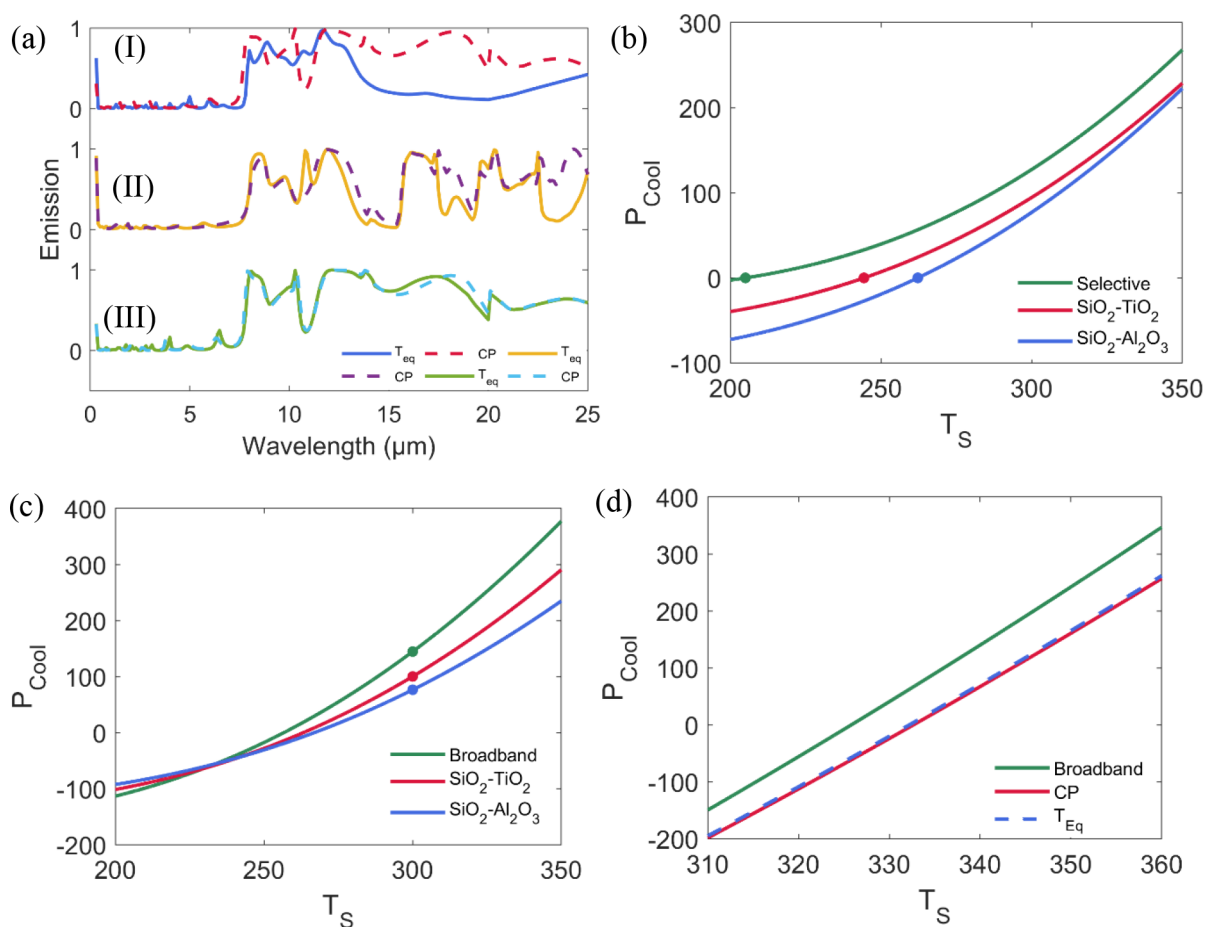
Trends are different for increasing  $h_c$  for a fixed  $T_{Amb}$  compared to fixed  $h_c$  for rising  $T_{Amb}$ . As seen in Figure 4(b),  $P_{Crit}$  becomes lower with increasing  $h_c$ . When there is no significant heat load acting on the system, the surface can maintain its low temperature, as shown when  $h_c \approx q_i \approx 0$ . However, with increasing  $h_c$ , the surface starts to interact with its environment. As  $h_c$  increases, the heat exchange rate will be higher and will dominate the radiative heat exchange mechanism, and  $T_{Eq}$  will converge to  $T_{Amb}$  when  $h_c \gg 0$ . With increasing the heat exchange rate, the heat load acting on the surface will increase; therefore, the switch from a selective to broadband profile occurs earlier with  $q_i$  as seen in Figure 4(b). Besides, due to the dominance of the nonradiative heat exchange, the performances of the different emission profiles become indifferent. This indicates that in the presence of strong nonradiative heat exchange one may not have any

**Table 1. Corresponding Power and Average Reflection Percentages for Structures with Different Material Pairs, Designed for CP Maximization and  $T_{Eq}$  Minimization**

Target	Material pair	Power ( $\text{Wm}^{-2}$ )		Avg. Reflection ( $\bar{R}(\lambda)$ )			
		$P_{Rad}$	$P_{Sun}$	$P_{Atm}$	$\bar{R}_I (\lambda_I)$ (%)	$\bar{R}_{II} (\lambda_{II})$ (%)	$\bar{R}_{III} (\lambda_{III})$ (%)
CP	TiO <sub>2</sub> -SiO <sub>2</sub>	242	13.23	140.61	91.5	25.8	29.8
CP	Al <sub>2</sub> O <sub>3</sub> -SiO <sub>2</sub>	204	25.71	101.77	93.5	29.4	37.7
$T_{Eq}$	TiO <sub>2</sub> -SiO <sub>2</sub>	61.94	7.74	54.2	95.1	27.7	70.2
$T_{Eq}$	Al <sub>2</sub> O <sub>3</sub> -SiO <sub>2</sub>	100.39	22.24	78.15	94	28.8	56.5

**Table 2. Layer Thicknesses in Coatings Designed for CP Maximization and  $T_{Eq}$  Minimization with Different Material Pairs for Varying Conditions**

	$h_c = 0, q = 0$				$h_c = 5 \text{ Wm}^{-2} \text{ K}^{-1}, q = 400 \text{ Wm}^{-2}$			
	Max CP		Min $T_{Eq}$		Max CP		Min $T_{Eq}$	
TiO <sub>2</sub>	0.19	2.92	Al <sub>2</sub> O <sub>3</sub>	0.16	0.50	TiO <sub>2</sub>	0.21	0.25
SiO <sub>2</sub>	2.52	0.59	SiO <sub>2</sub>	1.17	1.32	SiO <sub>2</sub>	2.62	2.14
TiO <sub>2</sub>	0.07	2.50	Al <sub>2</sub> O <sub>3</sub>	1.32	1.18	TiO <sub>2</sub>	0.13	0.26
SiO <sub>2</sub>	2.53	1.79	SiO <sub>2</sub>	2.60	1.931	SiO <sub>2</sub>	2.77	2.99
Ag	0.1	0.1	Ag	0.1	0.1	Ag	0.1	0.1

**Figure 6.** (a) Calculated spectra for the structures: (I) SiO<sub>2</sub>-TiO<sub>2</sub> pair designed for  $T_{Eq}$  minimization and CP maximization. (II) SiO<sub>2</sub>-Al<sub>2</sub>O<sub>3</sub> pair designed for  $T_{Eq}$  minimization and CP maximization. (III) SiO<sub>2</sub>-TiO<sub>2</sub> pairs designed for  $T_{Eq}$  minimization and CP maximization for  $h_c = 5 \text{ Wm}^{-2} \text{ K}^{-1}$  and  $q = 400 \text{ Wm}^{-2}$ . (b)  $T_s$ - $P_{Cool}$  curves for the structures designed to minimize  $T_{Eq}$  and selective profile. (c)  $T_s$ - $P_{Cool}$  curves for the structures designed to maximize  $P_{Cool}$  and broadband profile. (d)  $T_s$ - $P_{Cool}$  curves for the structure with SiO<sub>2</sub>-TiO<sub>2</sub> pair designed to minimize  $T_{Eq}$  and maximize CP.

benefit at all from radiative cooling. Therefore, it is highly crucial to consider the nonradiative cooling mechanisms used in the system of interest at which radiative cooling coatings are going to be implemented.

As seen in the results shown in Figure 4,  $T_{Eq}$  values remained around 300 K levels and reached their maximum when  $q$  becomes  $250 \text{ Wm}^{-2}$ . Thermal radiation at such temperatures is mostly confined in the 8–13  $\mu\text{m}$  wavelength interval, with

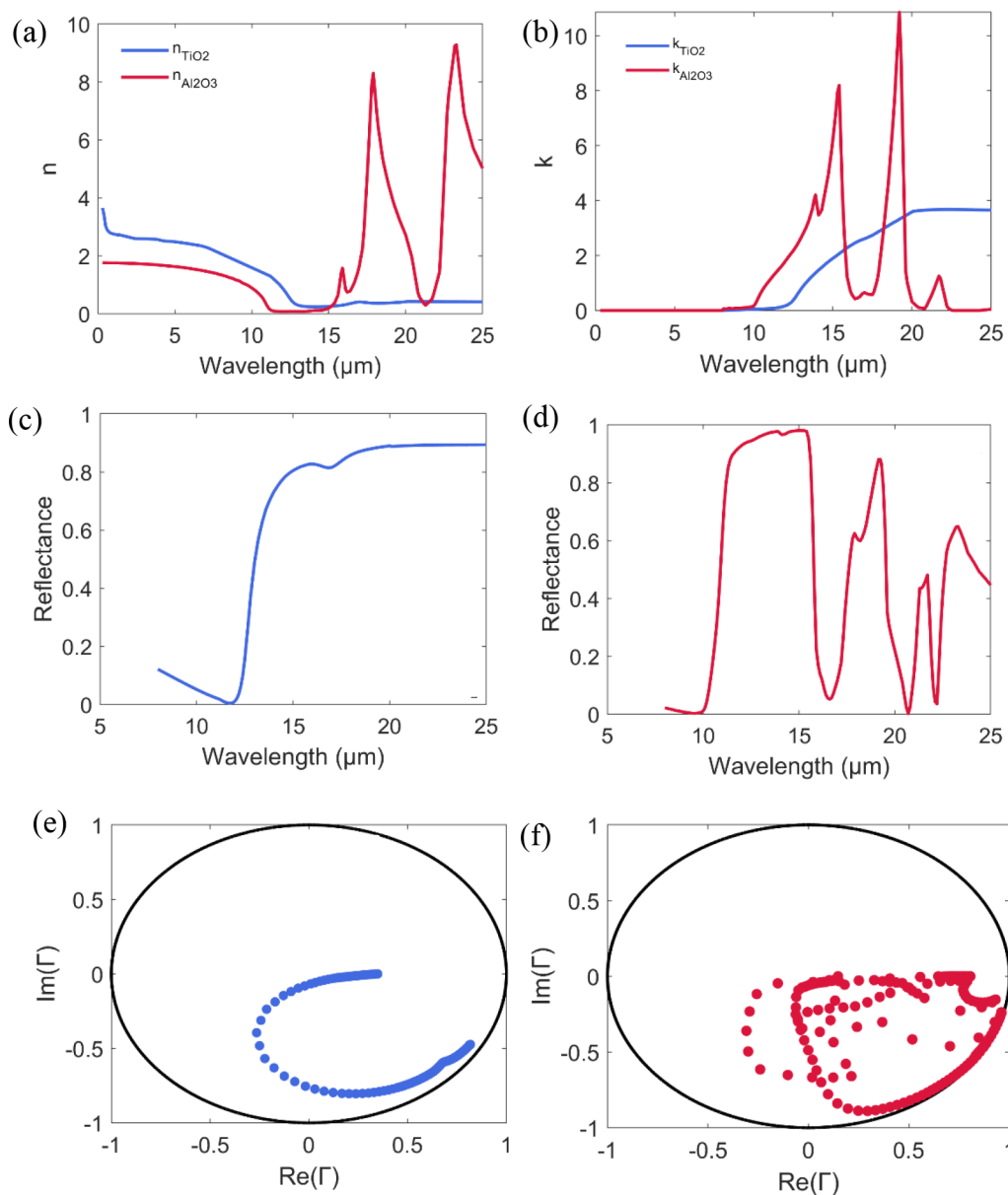


**Figure 7.** (a) Real parts of the refractive indices of  $\text{TiO}_2$  and  $\text{Al}_2\text{O}_3$ . (b) Imaginary parts of the refractive indices of  $\text{TiO}_2$  and  $\text{Al}_2\text{O}_3$ . (c) Reflection of single  $\text{TiO}_2$  medium. (d) Reflection of single  $\text{Al}_2\text{O}_3$  medium. (e) Reflection coefficients of  $\text{TiO}_2$  on complex reflection plane. (f) Reflection coefficients of  $\text{Al}_2\text{O}_3$  on complex reflection plane.

relatively smaller contributions from shorter wavelengths. Therefore, the impact of emission at those shorter wavelengths on  $T_{Eq}$  is limited. However, at further elevated temperatures which can be achieved with higher  $q$ , the contribution from radiation at shorter wavelengths than  $8 \mu\text{m}$  has considerable influence on the  $T_{Eq}$ . Therefore, emissivity profiles with unity emission starting from as low as  $2.5 \mu\text{m}$  can provide significantly lower  $T_{Eq}$  than the broadband profile demonstrated above (with unity emission starting from  $8 \mu\text{m}$ ). When corresponding  $T_{Eq}$  values with increasing  $q$  for the profiles, depicted in Figure 5(a), have different starting points of unity emission, the impact of bandwidth of the unity emission on  $T_{Eq}$  can be better understood. As seen in Figure 5(b), the profile broadband II results in lower  $T_{Eq}$  values compared to the selective and broadband profiles when  $q$  becomes higher than  $150 \text{ Wm}^{-2}$ , and the difference increases as  $q$  increases. When  $q$  reaches to  $4 \times 10^4 \text{ Wm}^{-2}$  levels, the broadband III profile

becomes more superior than broadband II in terms of  $T_{Eq}$ . At such elevated temperatures, radiation emitted from the surface becomes even higher than the incident solar irradiance, which makes emission of thermal radiation even at the visible spectrum more advantageous. These analyses demonstrate the importance of the bandwidth of the unity emission depending on the total heat load acting on the system.

#### 4. REALIZATION OF EMISSION PROFILES

For realization of the discussed spectral emissivity profiles, we designed multilayer structures with different material combinations to maximize  $P_{Cool}(T)$  and minimize  $T_{Eq}$  without predetermined spectral emission profiles. To achieve this, we used the method we previously proposed in ref 53. The layer numbers of the structures are fixed to 4, and thicknesses of alternating layers are used and optimized on top of a 100 nm Ag layer.  $\text{SiO}_2\text{-TiO}_2$  and  $\text{SiO}_2\text{-Al}_2\text{O}_3$  pairs are used as layer

materials, which are among commonly used materials in radiative cooling coatings.<sup>2,52,53</sup> The optical properties for SiO<sub>2</sub>, Al<sub>2</sub>O<sub>3</sub> and TiO<sub>2</sub> are retrieved from refs 160 and 161. Thicknesses for each designed coating with corresponding materials and conditions are listed in Table 2. Note that small  $k$  values in the visible and near-infrared spectra may result in considerable absorption of the solar irradiance and degrades the radiative cooling performance. However, such an outcome can be avoided by keeping layer thicknesses small, e.g., on the order of few micrometers, as seen in Tables 1 and 2. In Figure 6(a), spectral emission profiles when  $h_c = 0$  and  $q_i = 0$  are demonstrated for  $P_{Cool}(T)$  maximization and  $T_{Eq}$  minimization with different material pairs. As shown in Figure 6(a), the spectral profiles are similar for  $\lambda < 13 \mu\text{m}$ . However, for the spectral region  $\lambda > 13 \mu\text{m}$ , emission starts to decrease considerably for the structure optimized for  $T_{Eq}$  minimization, whereas it remains high for the structure optimized for  $P_{Cool}(T)$  maximization for SiO<sub>2</sub>–TiO<sub>2</sub> pairs. Change in emissivity is not as strong as in the case of SiO<sub>2</sub>–TiO<sub>2</sub> pairs, when SiO<sub>2</sub>–Al<sub>2</sub>O<sub>3</sub> pairs are used. Corresponding  $P_{Rad}$ ,  $P_{Sun}$ , and  $P_{Atm}$  together with the average emission values are shown in Table 1. As depicted in Table 1, the total radiative heat load due to  $P_{Sun}$  and  $P_{Atm}$  is increased by 38 Wm<sup>−2</sup>, from 62 to 100 Wm<sup>−2</sup>, when TiO<sub>2</sub> is substituted by Al<sub>2</sub>O<sub>3</sub>. Such change stems from changes in average reflectivity in 0.3–8 and 13–25  $\mu\text{m}$ . Even a 1% change in average reflection in 0.3–8  $\mu\text{m}$  caused an increase of 15 Wm<sup>−2</sup> in  $P_{Sun}$  and a 15% average reflection change in 13–25  $\mu\text{m}$  results in an approximate 25 Wm<sup>−2</sup> raise in  $P_{Atm}$ . Despite these changes, average reflection in the 8–13  $\mu\text{m}$  range remained similar for these two structures; thus, additional heat load cannot be compensated with higher thermal radiation emission in the 8–13  $\mu\text{m}$  spectrum, and higher  $T_{Eq}$  is observed when Al<sub>2</sub>O<sub>3</sub> is used instead of TiO<sub>2</sub>. Based on the corresponding  $T_s$ – $P_{Cool}$  curves depicted in Figure 6(b),  $T_{Eq}$  values of 244 and 262 K are achieved for SiO<sub>2</sub>–TiO<sub>2</sub> and SiO<sub>2</sub>–Al<sub>2</sub>O<sub>3</sub> pairs, respectively. These results emphasize the importance of material selection on  $T_{Eq}$ , which can cause approximately 20 K difference in  $T_{Eq}$ . It is important to note that  $T_{Eq}$  for the selective profile is around 205 K indicating that by further reducing the heat load even lower  $T_{Eq}$  values can be achieved.

When  $P_{Cool}(T_s = 300 \text{ K})$  is of interest but not the  $T_{Eq}$  minimization, the calculated final spectrum of the structure with SiO<sub>2</sub>–TiO<sub>2</sub> pairs has changed from selective to broadband, to increase the  $P_{Rad}$  by emitting thermal radiation at  $\lambda > 13 \mu\text{m}$ . As seen in Figure 6(a), a drastic change is observed in the spectra, whereas it is not the case for the structure with SiO<sub>2</sub>–Al<sub>2</sub>O<sub>3</sub> pairs. As tabulated in Table 1, the change in average reflectivity is around 40% for the former, whereas it is 20% for the latter. Final  $P_{Cool}(T_s = 300 \text{ K})$  is equal to 100 and 75 Wm<sup>−2</sup> for the structures with SiO<sub>2</sub>–TiO<sub>2</sub> and SiO<sub>2</sub>–Al<sub>2</sub>O<sub>3</sub>, respectively, and it is approximately 140 Wm<sup>−2</sup> for the broadband profile, as shown in Figure 6(c). Finally, when the structure is designed to maximize  $P_{Cool}$  and minimize  $T_{Eq}$  when  $h_c \gg 0$  and  $q_i \gg 0$  with SiO<sub>2</sub>–TiO<sub>2</sub> pairs, spectra shown in Figure 6(a) are achieved. As seen, no significant changes in the spectra are observed and corresponding  $T_s$ – $P_{Cool}$  becomes indifferent. There is an 8 K difference in  $T_{Eq}$  for the broadband and the achieved profiles.

The differences between the observed outcomes for the structures with SiO<sub>2</sub>–TiO<sub>2</sub> and SiO<sub>2</sub>–Al<sub>2</sub>O<sub>3</sub> are related to differences between the optical properties between TiO<sub>2</sub> and Al<sub>2</sub>O<sub>3</sub>. First, due to the refractive index differences in visible

and near-infrared spectra,<sup>59</sup> as depicted in Figure 7(a), there are slight differences between the average reflectivity at these spectra, which causes an increase in  $P_{Sun}$  up to 15–20 Wm<sup>−2</sup> and leading to reduction in  $P_{Cool}$  and raise in  $T_{Eq}$ . As given in Table 1, the second major difference occurs at  $\lambda > 13 \mu\text{m}$ , where the real and imaginary parts of the refractive indices,  $n$  and  $k$ , respectively, of TiO<sub>2</sub> and Al<sub>2</sub>O<sub>3</sub> are drastically different.<sup>59</sup> Such differences in fact provide a good example to demonstrate the role of dispersion in optical properties of coating materials. Al<sub>2</sub>O<sub>3</sub> has strong absorption peaks around 17 and 22  $\mu\text{m}$  wavelengths, shown in Figure 7(d), which occurs due the sudden changes in both  $n$  and  $k$  of Al<sub>2</sub>O<sub>3</sub>. On the other hand,  $n$  and  $k$  of TiO<sub>2</sub> is free of such resonance-like changes as seen in Figure 7(a) and (b); therefore, it exhibits near constant reflectivity after 15  $\mu\text{m}$  as depicted in Figure 7(c). Due to such dispersive characteristics of Al<sub>2</sub>O<sub>3</sub>, it is challenging to suppress such absorption modes and satisfy high reflection at  $\lambda > 13 \mu\text{m}$  for  $T_{Eq}$  minimization, with the structure in consideration. In other words, required thicknesses to satisfy near-perfect impedance mismatch at 17 and 22  $\mu\text{m}$  are significantly different than adjacent wavelengths due to the dispersion in Al<sub>2</sub>O<sub>3</sub>. Such differences can be visualized by considering reflection coefficients,  $\Gamma(\lambda > 13 \mu\text{m})$ , of Al<sub>2</sub>O<sub>3</sub> and TiO<sub>2</sub> as seen in Figure 7(e) and (f). As seen, distribution of  $\Gamma(\lambda > 13 \mu\text{m})$  of Al<sub>2</sub>O<sub>3</sub> is more dispersed compared to  $\Gamma(\lambda > 13 \mu\text{m})$  of TiO<sub>2</sub>, due to the difference in dispersion in optical properties of these materials. Because of this property of Al<sub>2</sub>O<sub>3</sub>, it is relatively more difficult to achieve broadband reflection at  $\lambda > 13 \mu\text{m}$  with pairs of Al<sub>2</sub>O<sub>3</sub>–SiO<sub>2</sub> compared to pairs of TiO<sub>2</sub>–SiO<sub>2</sub>, which leads to poorer performance in achieving selective emission profiles, thus lower  $T_{Eq}$ .

The dispersion characteristics of Al<sub>2</sub>O<sub>3</sub> at  $\lambda > 13 \mu\text{m}$  are also the source of high average reflectivity which leads to lower  $P_{Cool}$  when  $h_c \approx q_i \approx 0$  or higher  $T_{Eq}$  when  $h_c \gg 0$  and  $q_i \gg 0$  with the structure composed of Al<sub>2</sub>O<sub>3</sub>–SiO<sub>2</sub> pairs. A similar challenge in achieving broadband reflection at  $\lambda > 13 \mu\text{m}$  due to the dispersion of Al<sub>2</sub>O<sub>3</sub> also exists when broadband absorption/emission is desired. At this wavelength interval, although Al<sub>2</sub>O<sub>3</sub> has higher absorption on average due to several absorption modes, increasing the absorption at nonhighly absorbing wavelengths while preserving the high absorption at adjacent wavelengths is challenging due to differences in  $\Gamma(\lambda)$ . Due to weak dispersion characteristics in  $n$  and  $k$  of TiO<sub>2</sub>, achieving impedance matching in the broadband spectrum is simpler in the case of TiO<sub>2</sub>–SiO<sub>2</sub> pairs; thus, higher  $P_{Cool}$  or lower  $T_{Eq}$  is achieved when  $h_c \approx q_i \approx 0$  or  $h_c \gg 0$ ,  $q_i \gg 0$ , respectively.

## 5. CONCLUSIONS AND REMARKS

Spectral requirements for radiative cooling may vary in the presence of heat generation or weak thermal isolation from the environment. It was shown that, as the heat load increases in the system, drastic changes in the *ideal* emission profile occur. In recent years, many types of coatings have been proposed and designed with spectral emission profiles that are very close to the selective emission profile. As the efficiency of the radiative cooling is demonstrated with experimental measurements below ambient air temperature under direct sunlight, research toward applicability of those coatings in large scale is accelerated. Although such a selective profile is better for achieving  $T_{Eq}$  below ambient temperature under extreme isolation, it is not the most appropriate profile for real applications at which such extreme isolation may not be

realistic. Therefore, it is equally important to seek coatings that are closer to the broadband profile while studying the applicability of radiative cooling coatings in large scale.

It is well-known that any type of coating's spectral characteristics is controlled by the material it is composed of and geometrical dimensions of the features it has. Usually, in most of the radiative cooling coatings, a metallic back reflector is used for broadband reflection, preventing solar irradiance and atmospheric thermal radiation absorption. Thermal radiation emission from the surface requirement is fulfilled by the materials which have strong absorption at radiation wavelengths, typically  $\lambda > 8 \mu\text{m}$ . It was also shown that both reflection of solar irradiance and thermal emission from the surface requirements can be simultaneously satisfied by utilizing micro/nanoparticle-embedded polymers through tailoring of scattering from the particles by control of their distribution inside the host polymer. Yet, most of the recent literature is focused on cooling below ambient temperature and uses the selective emission profile, but not the broadband emission profile, which is shown to be more appropriate for cooling at temperatures above ambient. Therefore, analysis of coating characteristics at wavelengths longer than  $13 \mu\text{m}$  is crucial.

In addition, when the radiative cooling coating is not treated as a stand-alone system, requirements of the system that the radiative cooler is going to be integrated with comes into the picture, such as aesthetic, thermal, and electromagnetic. For instance, surface color becomes highly important when the coating is going to be integrated for use in cooling of buildings, which requires modifications of the coatings' spectral characteristics in the visible spectrum. Many coatings have been proposed under the topic of colorful radiative cooling; however, their characteristics at  $\lambda > 13 \mu\text{m}$  are not explored in detail, which may require adjustments depending on the operating conditions. Besides the color, the applied coating should not reduce the performance of the other cooling or thermal isolation mechanisms. Cooling with either natural or forced convection is a widely utilized approach and proven to be effective. Therefore, materials of the radiative cooler should be chosen in accordance with the convective mechanisms.

Finally, the radiative cooling coating must comply with the systems' electromagnetic requirements that it is going to be integrated with. Some examples of such systems include solar cells, which harvest energy from visible and near-infrared spectra, and telecommunication systems, which receive and transmit microwave/RF signals. Therefore, any radiative cooling materials should be chosen by considering their electromagnetic properties at different portions of the electromagnetic spectrum of interest. All types of these additional requirements bring extra constraints that should be addressed during the design stage of the radiative cooler. Considering the significant progress made in the field of radiative cooling and advancements in micro/nanotechnology, knowledge in the field is mature enough to be extended to application-dependent development of feasible radiative cooling structures.

## AUTHOR INFORMATION

### Corresponding Author

Kursat Sendur – Faculty of Engineering and Natural Science, Sabanci University, Istanbul 34956, Turkey; [orcid.org/](https://orcid.org/)

0000-0003-3210-7542; Email: [kursat.sendur@sabanciuniv.edu](mailto:kursat.sendur@sabanciuniv.edu)

## Authors

Muhammed Ali Kecebas – Faculty of Engineering and Natural Science, Sabanci University, Istanbul 34956, Turkey  
Pinar Menguc – Center for Energy, Environment and Economy, Ozyegin University, Istanbul 34794, Turkey

Complete contact information is available at: <https://pubs.acs.org/10.1021/acsaoam.3c00092>

## Funding

This material is based upon work supported by the Air Force Office of Scientific Research (Aerospace Materials for Extreme Environments Program, PM: Dr. Ali Sayir) under award number FA8655-22-1-7023.

## Notes

The authors declare no competing financial interest.

## REFERENCES

- (1) Catalanotti, S.; Cuomo, V.; Piro, G.; Ruggi, D.; Silvestrini, V.; Troise, G. The radiative cooling of selective surfaces. *Sol. Energy* **1975**, *17* (2), 83–89.
- (2) Raman, A. P.; Anoma, M. A.; Zhu, L.; Rephaeli, E.; Fan, S. Passive radiative cooling below ambient air temperature under direct sunlight. *Nature* **2014**, *515* (7528), 540–544.
- (3) Howell, J. R.; Mengüç, M. P.; Daun, K.; Siegel, R. *Thermal Radiation Heat Transfer*; CRC Press, 2020.
- (4) Idso, S. B.; Jackson, R. D. Thermal radiation from the atmosphere. *Journal of geophysical research* **1969**, *74* (23), 5397–5403.
- (5) Zhao, B.; Hu, M.; Ao, X.; Chen, N.; Pei, G. Radiative cooling: A review of fundamentals, materials, applications, and prospects. *Applied energy* **2019**, *236*, 489–513.
- (6) Li, Z.; Chen, Q.; Song, Y.; Zhu, B.; Zhu, J. Fundamentals, materials, and applications for daytime radiative cooling. *Advanced Materials Technologies* **2020**, *5* (5), 1901007.
- (7) Goyal, A. K.; Kumar, A. Recent advances and progresses in photonic devices for passive radiative cooling application: a review. *Journal of Nanophotonics* **2020**, *14* (3), 030901–030901.
- (8) Yin, X.; Yang, R.; Tan, G.; Fan, S. Terrestrial radiative cooling: Using the cold universe as a renewable and sustainable energy source. *Science* **2020**, *370* (6518), 786–791.
- (9) Hossain, M. M.; Gu, M. Radiative cooling: principles, progress, and potentials. *Advanced Science* **2016**, *3* (7), 1500360.
- (10) Yu, X.; Chan, J.; Chen, C. Review of radiative cooling materials: Performance evaluation and design approaches. *Nano Energy* **2021**, *88*, 106259.
- (11) Bijarniya, J. P.; Sarkar, J.; Maiti, P. Review on passive daytime radiative cooling: Fundamentals, recent researches, challenges and opportunities. *Renewable and Sustainable Energy Reviews* **2020**, *133*, 110263.
- (12) Zeyghami, M.; Goswami, D. Y.; Stefanakos, E. A review of clear sky radiative cooling developments and applications in renewable power systems and passive building cooling. *Sol. Energy Mater. Sol. Cells* **2018**, *178*, 115–128.
- (13) Sato, D.; Yamada, N. Review of photovoltaic module cooling methods and performance evaluation of the radiative cooling method. *Renewable and Sustainable Energy Reviews* **2019**, *104*, 151–166.
- (14) Ahmed, S.; Li, Z.; Javed, M. S.; Ma, T. A review on the integration of radiative cooling and solar energy harvesting. *Materials Today Energy* **2021**, *21*, 100776.
- (15) Chen, J.; Lu, L. Development of radiative cooling and its integration with buildings: A comprehensive review. *Sol. Energy* **2020**, *212*, 125–151.
- (16) Lu, X.; Xu, P.; Wang, H.; Yang, T.; Hou, J. Cooling potential and applications prospects of passive radiative cooling in buildings:

The current state-of-the-art. *Renewable and Sustainable Energy Reviews* **2016**, *65*, 1079–1097.

(17) Li, W.; Li, Y.; Shah, K. W. A materials perspective on radiative cooling structures for buildings. *Sol. Energy* **2020**, *207*, 247–269.

(18) Chen, L.; Zhang, K.; Ma, M.; Tang, S.; Li, F.; Niu, X. Sub-ambient radiative cooling and its application in buildings. *Building Simulation* **2020**, *13*, 1165–1189.

(19) Pirvaram, A.; Talebzadeh, N.; Leung, S. N.; O'Brien, P. G. Radiative cooling for buildings: A review of techno-enviro-economics and life-cycle assessment methods. *Renewable and Sustainable Energy Reviews* **2022**, *162*, 112415.

(20) Suhendri, H.; Hu, M.; Su, Y.; Darkwa, J.; Riffat, S. Implementation of passive radiative cooling technology in buildings: A review. *Buildings* **2020**, *10* (12), 215.

(21) Hanif, M.; Mahlia, T. M. I.; Zare, A.; Saksahdan, T. J.; Metselaar, H. S. C. Potential energy savings by radiative cooling system for a building in tropical climate. *Renewable and sustainable energy reviews* **2014**, *32*, 642–650.

(22) Zhang, J.; Yuan, J.; Liu, J.; Zhou, Z.; Sui, J.; Xing, J.; Zuo, J. Cover shields for sub-ambient radiative cooling: A literature review. *Renewable and Sustainable Energy Reviews* **2021**, *143*, 110959.

(23) Liu, J.; Zhang, J.; Zhang, D.; Jiao, S.; Xing, J.; Tang, H.; Zhang, Y.; Li, S.; Zhou, Z.; Zuo, J. Sub-ambient radiative cooling with wind cover. *Renewable and Sustainable Energy Reviews* **2020**, *130*, 109935.

(24) Vilà, R.; Martorell, I.; Medrano, M.; Castell, A. Adaptive covers for combined radiative cooling and solar heating. A review of existing technology and materials. *Sol. Energy Mater. Sol. Cells* **2021**, *230*, 111275.

(25) Wang, J.; Tan, G.; Yang, R.; Zhao, D. Materials, structures, and devices for dynamic radiative cooling. *Cell Reports Physical Science* **2022**, *3*, 101198.

(26) An, Y.; Fu, Y.; Dai, J. G.; Yin, X.; Lei, D. Switchable radiative cooling technologies for smart thermal management. *Cell Reports Physical Science* **2022**, *3* (10), 101098.

(27) Taylor, S.; Long, L.; McBurney, R.; Sabbaghi, P.; Chao, J.; Wang, L. Spectrally-selective vanadium dioxide based tunable metafilm emitter for dynamic radiative cooling. *Sol. Energy Mater. Sol. Cells* **2020**, *217*, 110739.

(28) Xu, X.; Gu, J.; Zhao, H.; Zhang, X.; Dou, S.; Li, Y.; Zhao, J.; Zhan, Y.; Li, X. Passive and dynamic phase-change-based radiative cooling in outdoor weather. *ACS Appl. Mater. Interfaces* **2022**, *14* (12), 14313–14320.

(29) Wang, S.; Jiang, T.; Meng, Y.; Yang, R.; Tan, G.; Long, Y. Scalable thermochromic smart windows with passive radiative cooling regulation. *Science* **2021**, *374* (6574), 1501–1504.

(30) Taylor, S.; Yang, Y.; Wang, L. Vanadium dioxide based Fabry-Perot emitter for dynamic radiative cooling applications. *Journal of Quantitative Spectroscopy and Radiative Transfer* **2017**, *197*, 76–83.

(31) Butler, A.; Argyropoulos, C. Mechanically tunable radiative cooling for adaptive thermal control. *Applied Thermal Engineering* **2022**, *211*, 118527.

(32) Liu, J.; Zhou, Z.; Zhang, J.; Feng, W.; Zuo, J. Advances and challenges in commercializing radiative cooling. *Materials Today Physics* **2019**, *11*, 100161.

(33) Cui, Y.; Luo, X.; Zhang, F.; Sun, L.; Jin, N.; Yang, W. Progress of passive daytime radiative cooling technologies towards commercial applications. *Particuology* **2022**, *67*, 57–67.

(34) Jeon, S.; Shin, J. Ideal spectral emissivity for radiative cooling of earthbound objects. *Sci. Rep.* **2020**, *10* (1), 13038.

(35) Fan, S.; Li, W. Photonics and thermodynamics concepts in radiative cooling. *Nat. Photonics* **2022**, *16* (3), 182–190.

(36) Chen, Z.; Zhu, L.; Raman, A.; Fan, S. Radiative cooling to deep sub-freezing temperatures through a 24-h day-night cycle. *Nat. Commun.* **2016**, *7* (1), 13729.

(37) Chamoli, S. K.; Li, W.; Guo, C.; ElKabbash, M. Angularly selective thermal emitters for deep subfreezing daytime radiative cooling. *Nanophotonics* **2022**, *11* (16), 3709–3717.

(38) Lin, S. Y.; Fleming, J. G.; Chow, E.; Bur, J.; Choi, K. K.; Goldberg, A. Enhancement and suppression of thermal emission by a three-dimensional photonic crystal. *Phys. Rev. B* **2000**, *62* (4), R2243.

(39) Schuller, J. A.; Taubner, T.; Brongersma, M. L. Optical antenna thermal emitters. *Nat. Photonics* **2009**, *3* (11), 658–661.

(40) Greffet, J. J. Controlled incandescence. *Nature* **2011**, *478* (7368), 191–192.

(41) Narayanaswamy, A.; Chen, G. Thermal emission control with one-dimensional metalodielectric photonic crystals. *Phys. Rev. B* **2004**, *70* (12), 125101.

(42) Celanovic, I.; Perreault, D.; Kassakian, J. Resonant-cavity enhanced thermal emission. *Phys. Rev. B* **2005**, *72* (7), 075127.

(43) Rephaeli, E.; Fan, S. Absorber and emitter for solar thermophotovoltaic systems to achieve efficiency exceeding the Shockley-Queisser limit. *Opt. Express* **2009**, *17* (17), 15145–15159.

(44) Le Gall, J.; Olivier, M.; Greffet, J. J. Experimental and theoretical study of reflection and coherent thermal emission by a SiC grating supporting a surface-phonon polariton. *Phys. Rev. B* **1997**, *55* (15), 10105.

(45) Luo, C.; Narayanaswamy, A.; Chen, G.; Joannopoulos, J. D. Thermal radiation from photonic crystals: a direct calculation. *Phys. Rev. Lett.* **2004**, *93* (21), 213905.

(46) Chan, D. L.; Soljačić, M.; Joannopoulos, J. D. Thermal emission and design in 2D-periodic metallic photonic crystal slabs. *Opt. Express* **2006**, *14* (19), 8785–8796.

(47) Fleming, J. G.; Lin, S. Y.; El-Kady, L.; Biswas, R.; Ho, K. M. All-metallic three-dimensional photonic crystals with a large infrared bandgap. *Nature* **2002**, *417* (6884), 52–55.

(48) Rephaeli, E.; Fan, S. Tungsten black absorber for solar light with wide angular operation range. *Applied Physics Letters* **2008**, *92* (21), 211107.

(49) Arpin, K. A.; Losego, M. D.; Cloud, A. N.; Ning, H.; Mallek, J.; Sergeant, N. P.; Zhu, L.; Yu, Z.; Kalanyan, B.; Parsons, G. N.; Girolami, G. S.; Abelson, J. R.; Fan, S.; Braun, P. V. Three-dimensional self-assembled photonic crystals with high temperature stability for thermal emission modification. *Nat. Commun.* **2013**, *4* (1), 2630.

(50) Wang, M.; Hu, C.; Pu, M.; Huang, C.; Zhao, Z.; Feng, Q.; Luo, X. Truncated spherical voids for nearly omnidirectional optical absorption. *Opt. Express* **2011**, *19* (21), 20642–20649.

(51) Zhang, S.; Li, Y.; Feng, G.; Zhu, B.; Xiao, S.; Zhou, L.; Zhao, L. Strong infrared absorber: surface-microstructured Au film replicated from black silicon. *Opt. Express* **2011**, *19* (21), 20462–20467.

(52) Kecebas, M. A.; Menguc, M. P.; Kosar, A.; Sendur, K. Passive radiative cooling design with broadband optical thin-film filters. *Journal of Quantitative Spectroscopy and Radiative Transfer* **2017**, *198*, 179–186.

(53) Kecebas, M. A.; Menguc, M. P.; Kosar, A.; Sendur, K. Spectrally selective filter design for passive radiative cooling. *JOSA B* **2020**, *37* (4), 1173–1182.

(54) Kim, M.; Seo, J.; Yoon, S.; Lee, H.; Lee, J.; Lee, B. J. Optimization and performance analysis of a multilayer structure for daytime radiative cooling. *Journal of Quantitative Spectroscopy and Radiative Transfer* **2021**, *260*, 107475.

(55) Shi, Y.; Li, W.; Raman, A.; Fan, S. Optimization of multilayer optical films with a memetic algorithm and mixed integer programming. *Acs Photonics* **2018**, *5* (3), 684–691.

(56) Guan, Q.; Raza, A.; Mao, S. S.; Vega, L. F.; Zhang, T. Machine Learning-Enabled Inverse Design of Radiative Cooling Film with On-Demand Transmissive Color. *ACS Photonics* **2023**, *10* (3), 715–726.

(57) Chae, D.; Kim, M.; Jung, P.-H.; Son, S.; Seo, J.; Liu, Y.; Lee, B. J.; Lee, H. Spectrally selective inorganic-based multilayer emitter for daytime radiative cooling. *ACS Appl. Mater. Interfaces* **2020**, *12* (7), 8073–8081.

(58) Ma, H.; Yao, K.; Dou, S.; Xiao, M.; Dai, M.; Wang, L.; Zhao, H.; Zhao, J.; Li, Y.; Zhan, Y. Multilayered SiO<sub>2</sub>/Si<sub>3</sub>N<sub>4</sub> photonic emitter to achieve high-performance all-day radiative cooling. *Sol. Energy Mater. Sol. Cells* **2020**, *212*, 110584.

- (59) Palik, E. D., Ed.; *Handbook of Optical Constants of Solids*, Vol. 3; Academic Press, 1998.
- (60) Jeong, S. Y.; Tso, C. Y.; Ha, J.; Wong, Y. M.; Chao, C. Y.; Huang, B.; Qiu, H. Field investigation of a photonic multi-layered TiO<sub>2</sub> passive radiative cooler in sub-tropical climate. *Renewable Energy* **2020**, *146*, 44–55.
- (61) Lee, G. J.; Kim, Y. J.; Kim, H. M.; Yoo, Y. J.; Song, Y. M. Colored, daytime radiative coolers with thin-film resonators for aesthetic purposes. *Advanced Optical Materials* **2018**, *6* (22), 1800707.
- (62) Tikhonravov, A. V.; Trubetskov, M. K.; DeBell, G. W. Application of the needle optimization technique to the design of optical coatings. *Applied Optics* **1996**, *35* (28), 5493–5508.
- (63) Vincent, P.; Cunha Sergio, G.; Jang, J.; Kang, I. M.; Park, J.; Kim, H.; Lee, M.; Bae, J.-H. Application of genetic algorithm for more efficient multi-layer thickness optimization in solar cells. *Energies* **2020**, *13* (7), 1726.
- (64) Kou, J. L.; Jurado, Z.; Chen, Z.; Fan, S.; Minnich, A. J. Daytime radiative cooling using near-black infrared emitters. *ACS Photonics* **2017**, *4* (3), 626–630.
- (65) Chae, D.; Lim, H.; So, S.; Son, S.; Ju, S.; Kim, W.; Rho, J.; Lee, H. Spectrally selective nanoparticle mixture coating for passive daytime radiative cooling. *ACS Appl. Mater. Interfaces* **2021**, *13* (18), 21119–21126.
- (66) Gangisetty, G.; Zevenhoven, R. A Review of Nanoparticle Material Coatings in Passive Radiative Cooling Systems Including Skylights. *Energies* **2023**, *16* (4), 1975.
- (67) Cheng, Z.; Shuai, Y.; Gong, D.; Wang, F.; Liang, H.; Li, G. Optical properties and cooling performance analyses of single-layer radiative cooling coating with mixture of TiO<sub>2</sub> particles and SiO<sub>2</sub> particles. *Science China Technological Sciences* **2021**, *64* (5), 1017–1029.
- (68) Huang, Z.; Ruan, X. Nanoparticle embedded double-layer coating for daytime radiative cooling. *International Journal of Heat and Mass Transfer* **2017**, *104*, 890–896.
- (69) Cheng, Z.; Wang, F.; Wang, H.; Liang, H.; Ma, L. Effect of embedded polydisperse glass microspheres on radiative cooling of a coating. *International Journal of Thermal Sciences* **2019**, *140*, 358–367.
- (70) Bao, H.; Yan, C.; Wang, B.; Fang, X.; Zhao, C. Y.; Ruan, X. Double-layer nanoparticle-based coatings for efficient terrestrial radiative cooling. *Sol. Energy Mater. Sol. Cells* **2017**, *168*, 78–84.
- (71) Huang, J.; Li, M.; Fan, D. Core-shell particles for devising high-performance full-day radiative cooling paint. *Applied Materials Today* **2021**, *25*, 101209.
- (72) Hu, D.; Sun, S.; Du, P.; Lu, X.; Zhang, H.; Zhang, Z. Hollow core-shell particle-containing coating for passive daytime radiative cooling. *Composites Part A: Applied Science and Manufacturing* **2022**, *158*, 106949.
- (73) Zhai, Y.; Ma, Y.; David, S. N.; Zhao, D.; Lou, R.; Tan, G.; Yang, R.; Yin, X. Scalable-manufactured randomized glass-polymer hybrid metamaterial for daytime radiative cooling. *Science* **2017**, *355* (6329), 1062–1066.
- (74) Ko, B.; Lee, D.; Badloe, T.; Rho, J. Metamaterial-based radiative cooling: towards energy-free all-day cooling. *Energies* **2019**, *12* (1), 89.
- (75) Kravets, V. G.; Kabashin, A. V.; Barnes, W. L.; Grigorenko, A. N. Plasmonic surface lattice resonances: a review of properties and applications. *Chem. Rev.* **2018**, *118* (12), 5912–5951.
- (76) Atwater, H. A.; Polman, A. Plasmonics for improved photovoltaic devices. *Nature Materials* **2010**, *9* (3), 205–213.
- (77) Utyushev, A. D.; Zakomirnyi, V. I.; Rasskazov, I. L. Collective lattice resonances: Plasmonics and beyond. *Reviews in Physics* **2021**, *6*, 100051.
- (78) Amendola, V.; Pilot, R.; Frascioni, M.; Maragò, O. M.; Iati, M. A. Surface plasmon resonance in gold nanoparticles: a review. *J. Phys.: Condens. Matter* **2017**, *29* (20), 203002.
- (79) Cherqui, C.; Bourgeois, M. R.; Wang, D.; Schatz, G. C. Plasmonic surface lattice resonances: Theory and computation. *Accounts of Chemical Research* **2019**, *52* (9), 2548–2558.
- (80) Rodriguez, S. R. K.; Abass, A.; Maes, B.; Janssen, O. T. A.; Vecchi, G.; Gomez Rivas, J. Coupling bright and dark plasmonic lattice resonances. *Physical Review X* **2011**, *1* (2), 021019.
- (81) Humphrey, A. D.; Barnes, W. L. Plasmonic surface lattice resonances on arrays of different lattice symmetry. *Phys. Rev. B* **2014**, *90* (7), 075404.
- (82) Rephaeli, E.; Raman, A.; Fan, S. Ultrabroadband photonic structures to achieve high-performance daytime radiative cooling. *Nano Lett.* **2013**, *13* (4), 1457–1461.
- (83) Choi, M.; Seo, J.; Yoon, S.; Nam, Y.; Lee, J.; Lee, B. J. All-day radiative cooling using a grating-patterned PDMS film emitter. *Applied Thermal Engineering* **2022**, *214*, 118771.
- (84) Seo, J.; Choi, M.; Lee, J.; Lee, B. J. Optimization of a grating structure in hexagonal array with omnidirectional emission for daytime radiative cooling. *Journal of Quantitative Spectroscopy and Radiative Transfer* **2022**, *284*, 108165.
- (85) Wong, R. Y.; Tso, C. Y.; Chao, C. Y.; Huang, B.; Wan, M. P. Ultra-broadband asymmetric transmission metallic gratings for subtropical passive daytime radiative cooling. *Sol. Energy Mater. Sol. Cells* **2018**, *186*, 330–339.
- (86) Long, L.; Yang, Y.; Wang, L. Simultaneously enhanced solar absorption and radiative cooling with thin silica micro-grating coatings for silicon solar cells. *Sol. Energy Mater. Sol. Cells* **2019**, *197*, 19–24.
- (87) Dai, Y.; Zhang, Z.; Ma, C. Radiative cooling with multilayered periodic grating under sunlight. *Opt. Commun.* **2020**, *475*, 126231.
- (88) Hervé, A.; Drévilion, J.; Ezzahri, Y.; Joulain, K. Radiative cooling by tailoring surfaces with microstructures: Association of a grating and a multi-layer structure. *Journal of Quantitative Spectroscopy and Radiative Transfer* **2018**, *221*, 155–163.
- (89) Hossain, M. M.; Jia, B.; Gu, M. A metamaterial emitter for highly efficient radiative cooling. *Adv. Opt. Mater.* **2015**, *3* (8), 1047–1051.
- (90) Cui, Y.; He, Y.; Jin, Y.; Ding, F.; Yang, L.; Ye, Y.; Zhong, S.; Lin, Y.; He, S. Plasmonic and metamaterial structures as electromagnetic absorbers. *Laser & Photonics Reviews* **2014**, *8* (4), 495–520.
- (91) Perrakis, G.; Tasolamprou, A. C.; Kenanakis, G.; Economou, E. N.; Tzortzakis, S.; Kafesaki, M. Combined nano and micro structuring for enhanced radiative cooling and efficiency of photovoltaic cells. *Sci. Rep.* **2021**, *11* (1), 11552.
- (92) Zhao, B.; Lu, K.; Hu, M.; Liu, J.; Wu, L.; Xu, C.; Xuan, Q.; Pei, G. Radiative cooling of solar cells with micro-grating photonic cooler. *Renewable Energy* **2022**, *191*, 662–668.
- (93) Zhu, L.; Raman, A.; Wang, K. X.; Anoma, M. A.; Fan, S. Radiative cooling of solar cells. *Optica* **2014**, *1* (1), 32–38.
- (94) Zhao, B.; Hu, M.; Ao, X.; Pei, G. Performance analysis of enhanced radiative cooling of solar cells based on a commercial silicon photovoltaic module. *Sol. Energy* **2018**, *176*, 248–255.
- (95) Gentle, A. R.; Smith, G. B. Is enhanced radiative cooling of solar cell modules worth pursuing? *Sol. Energy Mater. Sol. Cells* **2016**, *150*, 39–42.
- (96) Yalcin, R. A.; Blandre, E.; Joulain, K.; Drévilion, J. Colored radiative cooling coatings with nanoparticles. *ACS Photonics* **2020**, *7* (5), 1312–1322.
- (97) Xi, W.; Liu, Y.; Zhao, W.; Hu, R.; Luo, X. Colored radiative cooling: How to balance color display and radiative cooling performance. *International Journal of Thermal Sciences* **2021**, *170*, 107172.
- (98) Kim, H. H.; Im, E.; Lee, S. Colloidal photonic assemblies for colorful radiative cooling. *Langmuir* **2020**, *36* (23), 6589–6596.
- (99) Zhou, L.; Rada, J.; Song, H.; Ooi, B.; Yu, Z.; Gan, Q. Colorful surfaces for radiative cooling. *Journal of Photonics for Energy* **2021**, *11* (4), 042107–042107.
- (100) Son, S.; Jeon, S.; Chae, D.; Lee, S. Y.; Liu, Y.; Lim, H.; Oh, S. J.; Lee, H. Colored emitters with silica-embedded perovskite nanocrystals for efficient daytime radiative cooling. *Nano Energy* **2021**, *79*, 105461.
- (101) Zhu, W.; Droguet, B.; Shen, Q.; Zhang, Y.; Parton, T. G.; Shan, X.; Parker, R. M.; De Volder, M. F. L.; Deng, T.; Vignolini, S.;

- Li, T. Structurally colored radiative cooling cellulosic films. *Advanced Science* **2022**, *9* (26), 2202061.
- (102) Blandre, E.; Yalcin, R. A.; Joulain, K.; Drévilion, J. Microstructured surfaces for colored and non-colored sky radiative cooling. *Opt. Express* **2020**, *28* (20), 29703–29713.
- (103) Ding, Z.; Li, X.; Fan, X.; Xu, M.; Zhao, J.; Li, Y.; Xu, H. A review of the development of colored radiative cooling surfaces. *Carbon Capture Science & Technology* **2022**, *4*, 100066.
- (104) Zhai, H.; Fan, D.; Li, Q. Scalable and paint-format colored coatings for passive radiative cooling. *Sol. Energy Mater. Sol. Cells* **2022**, *245*, 111853.
- (105) Yalcin, R. A.; Blandre, E.; Joulain, K.; Drévilion, J. Colored radiative cooling coatings with fluorescence. *Journal of Photonics for Energy* **2021**, *11* (3), 032104–032104.
- (106) Min, S.; Jeon, S.; Yun, K.; Shin, J. All-color sub-ambient radiative cooling based on photoluminescence. *ACS Photonics* **2022**, *9* (4), 1196–1205.
- (107) Sheng, C.; An, Y.; Du, J.; Li, X. Colored radiative cooler under optical Tamm resonance. *ACS Photonics* **2019**, *6* (10), 2545–2552.
- (108) Lee, G. J.; Kim, Y. J.; Kim, H. M.; Yoo, Y. J.; Song, Y. M. Colored, daytime radiative coolers with thin-film resonators for aesthetic purposes. *Advanced Optical Materials* **2018**, *6* (22), 1800707.
- (109) Mandal, J.; Fu, Y.; Overvig, A. C.; Jia, M.; Sun, K.; Shi, N. N.; Zhou, H.; Xiao, X.; Yu, N.; Yang, Y. Hierarchically porous polymer coatings for highly efficient passive daytime radiative cooling. *Science* **2018**, *362* (6412), 315–319.
- (110) Xiang, B.; Zhang, R.; Luo, Y.; Zhang, S.; Xu, L.; Min, H.; Tang, S.; Meng, X. 3D porous polymer film with designed pore architecture and auto-deposited SiO<sub>2</sub> for highly efficient passive radiative cooling. *Nano Energy* **2021**, *81*, 105600.
- (111) Son, S.; Liu, Y.; Chae, D.; Lee, H. Cross-linked porous polymeric coating without a metal-reflective layer for sub-ambient radiative cooling. *ACS Appl. Mater. Interfaces* **2020**, *12* (52), 57832–57839.
- (112) Liu, J.; Tang, H.; Jiang, C.; Wu, S.; Ye, L.; Zhao, D.; Zhou, Z. Micro-Nano Porous Structure for Efficient Daytime Radiative Sky Cooling. *Adv. Funct. Mater.* **2022**, *32* (44), 2206962.
- (113) Chen, M.; Pang, D.; Mandal, J.; Chen, X.; Yan, H.; He, Y.; Yu, N.; Yang, Y. Designing mesoporous photonic structures for high-performance passive daytime radiative cooling. *Nano Lett.* **2021**, *21* (3), 1412–1418.
- (114) Sun, J.; Wang, J.; Guo, T.; Bao, H.; Bai, S. Daytime passive radiative cooling materials based on disordered media: A review. *Sol. Energy Mater. Sol. Cells* **2022**, *236*, 111492.
- (115) Li, D.; Liu, X.; Li, W.; Lin, Z.; Zhu, B.; Li, Z.; Li, J.; Li, B.; Fan, S.; Xie, J.; Zhu, J. Scalable and hierarchically designed polymer film as a selective thermal emitter for high-performance all-day radiative cooling. *Nat. Nanotechnol.* **2021**, *16* (2), 153–158.
- (116) Wang, T.; Wu, Y.; Shi, L.; Hu, X.; Chen, M.; Wu, L. A structural polymer for highly efficient all-day passive radiative cooling. *Nat. Commun.* **2021**, *12* (1), 365.
- (117) Mandal, J.; Yang, Y.; Yu, N.; Raman, A. P. Paints as a scalable and effective radiative cooling technology for buildings. *Joule* **2020**, *4* (7), 1350–1356.
- (118) Family, R.; Mengüç, M. P. Materials for radiative cooling: a review. *Procedia environmental sciences* **2017**, *38*, 752–759.
- (119) Eriksson, T. S.; Lushiku, E. M.; Granqvist, C. G. Materials for radiative cooling to low temperature. *Solar energy materials* **1984**, *11* (3), 149–161.
- (120) Pirouzfam, N.; Menguc, M. P.; Sendur, K. Colorization of passive radiative cooling coatings using plasmonic effects. *Sol. Energy Mater. Sol. Cells* **2023**, *253*, 112225.
- (121) Dou, S.; Xu, H.; Zhao, J.; Zhang, K.; Li, N.; Lin, Y.; Pan, L.; Li, Y. Bioinspired microstructured materials for optical and thermal regulation. *Adv. Mater.* **2021**, *33* (6), 2000697.
- (122) Fu, S. C.; Zhong, X. L.; Zhang, Y.; Lai, T. W.; Chan, K. C.; Lee, K. Y.; Chao, C. Y. Bio-inspired cooling technologies and the applications in buildings. *Energy and Buildings* **2020**, *225*, 110313.
- (123) Shi, N. N. *Biological and Bioinspired Photonic Materials for Passive Radiative Cooling and Waveguiding*. Ph.D. Thesis, Columbia University, 2018.
- (124) Yang, J.; Zhang, X.; Zhang, X.; Wang, L.; Feng, W.; Li, Q. Beyond the visible: bioinspired infrared adaptive materials. *Adv. Mater.* **2021**, *33* (14), 2004754.
- (125) Shi, N. N.; Tsai, C. C.; Camino, F.; Bernard, G. D.; Yu, N.; Wehner, R. Keeping cool: Enhanced optical reflection and radiative heat dissipation in Saharan silver ants. *Science* **2015**, *349* (6245), 298–301.
- (126) Shi, N. N.; Tsai, C. C.; Camino, F.; Bernard, G. D.; Wehner, R.; Yu, N. Radiative cooling nano-photonic structures discovered in saharan silver ants and related biomimetic metasurfaces. In *CLEO: QELS\_Fundamental Science*, San Jose, California, June 2016. DOI: 10.1364/CLEO\_QELS.2016.FTh3B.1.
- (127) Jeong, S. Y.; Tso, C. Y.; Wong, Y. M.; Chao, C. Y. FDTD simulations inspired by the daytime passive radiative cooling of the Sahara silver ant. In *Proceedings of 4th International Conference on Building Energy and Environment*, Melbourne, Australia, February 2018.
- (128) Wu, W.; Lin, S.; Wei, M.; Huang, J.; Xu, H.; Lu, Y.; Song, W. Flexible passive radiative cooling inspired by Saharan silver ants. *Sol. Energy Mater. Sol. Cells* **2020**, *210*, 110512.
- (129) Lin, S.; Ai, L.; Zhang, J.; Bu, T.; Li, H.; Huang, F.; Zhang, J.; Lu, Y.; Song, W. Silver ants-inspired flexible photonic architectures with improved transparency and heat radiation for photovoltaic devices. *Sol. Energy Mater. Sol. Cells* **2019**, *203*, 110135.
- (130) Li, T.; Zhai, Y.; He, S.; Gan, W.; Wei, Z.; Heidarinejad, M.; Dalgo, D.; Mi, R.; Zhao, X.; Song, J.; Dai, J.; Chen, C.; Aili, A.; Vellore, A.; Martini, A.; Yang, R.; Srebric, J.; Yin, X.; Hu, L. A radiative cooling structural material. *Science* **2019**, *364* (6442), 760–763.
- (131) Chowdhury, F. I.; Xu, Q.; Sinha, K.; Wang, X. Cellulose-upgraded polymer films for radiative sky cooling. *Journal of Quantitative Spectroscopy and Radiative Transfer* **2021**, *272*, 107824.
- (132) Gamage, S.; Banerjee, D.; Alam, M. M.; Hallberg, T.; Akerlind, C.; Sultana, A.; Shanker, R.; Berggren, M.; Crispin, X.; Kariis, H.; Zhao, D.; Jonsson, M. P. Reflective and transparent cellulose-based passive radiative coolers. *Cellulose* **2021**, *28* (14), 9383–9393.
- (133) Chen, X.; He, M.; Feng, S.; Xu, Z.; Peng, H.; Shi, S.; Liu, C.; Zhou, Y. Cellulose-based porous polymer film with auto-deposited TiO<sub>2</sub> as spectrally selective materials for passive daytime radiative cooling. *Opt. Mater.* **2021**, *120*, 111431.
- (134) Jaramillo-Fernandez, J.; Yang, H.; Schertel, L.; Whitworth, G. L.; Garcia, P. D.; Vignolini, S.; Sotomayor-Torres, C. M. Highly-scattering cellulose-based films for radiative cooling. *Advanced Science* **2022**, *9* (8), 2104758.
- (135) Chen, Y.; Dang, B.; Fu, J.; Wang, C.; Li, C.; Sun, Q.; Li, H. Cellulose-based hybrid structural material for radiative cooling. *Nano Lett.* **2021**, *21* (1), 397–404.
- (136) Tian, Y.; Shao, H.; Liu, X.; Chen, F.; Li, Y.; Tang, C.; Zheng, Y. Superhydrophobic and recyclable cellulose-fiber-based composites for high-efficiency passive radiative cooling. *ACS Appl. Mater. Interfaces* **2021**, *13* (19), 22521–22530.
- (137) Cheng, Z.; Han, H.; Wang, F.; Yan, Y.; Shi, X.; Liang, H.; Zhang, X.; Shuai, Y. Efficient radiative cooling coating with biomimetic human skin wrinkle structure. *Nano Energy* **2021**, *89*, 106377.
- (138) Lauster, T.; Mauer, A.; Herrmann, K.; Veitengruber, V.; Song, Q.; Senker, J.; Retsch, M. From Chitosan to Chitin: Bio-Inspired Thin Films for Passive Daytime Radiative Cooling. *Advanced Science* **2023**, *10*, 2206616.
- (139) Liu, B.-Y.; Xue, C.-H.; Zhong, H.-M.; Guo, X.-J.; Wang, H.-D.; Li, H.-G.; Du, M.-M.; Huang, M.-C.; Wei, R.-X.; Song, L.-G.; Chang, B.; Wang, Z. Multi-bioinspired self-cleaning energy-free cooling coatings. *Journal of Materials Chemistry A* **2021**, *9* (43), 24276–24282.
- (140) Yang, Z.; Sun, H.; Xi, Y.; Qi, Y.; Mao, Z.; Wang, P.; Zhang, J. Bio-inspired structure using random, three-dimensional pores in the

polymeric matrix for daytime radiative cooling. *Sol. Energy Mater. Sol. Cells* **2021**, *227*, 111101.

(141) Wang, S.; Wang, Y.; Zou, Y.; Chen, G.; Ouyang, J.; Jia, D.; Zhou, Y. Biologically inspired scalable-manufactured dual-layer coating with a hierarchical micropattern for highly efficient passive radiative cooling and robust superhydrophobicity. *ACS Appl. Mater. Interfaces* **2021**, *13* (18), 21888–21897.

(142) Jeong, S. Y.; Tso, C. Y.; Wong, Y. M.; Chao, C. Y.; Huang, B. Daytime passive radiative cooling by ultra emissive bio-inspired polymeric surface. *Sol. Energy Mater. Sol. Cells* **2020**, *206*, 110296.

(143) Yang, Z.; Zhang, J. Bioinspired radiative cooling structure with randomly stacked fibers for efficient all-day passive cooling. *ACS Appl. Mater. Interfaces* **2021**, *13* (36), 43387–43395.

(144) Yang, M.; Zou, W.; Guo, J.; Qian, Z.; Luo, H.; Yang, S.; Zhao, N.; Pattelli, L.; Xu, J.; Wiersma, D. S. Bioinspired “skin” with cooperative thermo-optical effect for daytime radiative cooling. *ACS Appl. Mater. Interfaces* **2020**, *12* (22), 25286–25293.

(145) Zhang, H.; Ly, K. C. S.; Liu, X.; Chen, Z.; Yan, M.; Wu, Z.; Wang, X.; Zheng, Y.; Zhou, H.; Fan, T. Biologically inspired flexible photonic films for efficient passive radiative cooling. *Proc. Natl. Acad. Sci. U. S. A.* **2020**, *117* (26), 14657–14666.

(146) Didari, A.; Mengüç, M. P. A biomimicry design for nanoscale radiative cooling applications inspired by *Morpho didius* butterfly. *Sci. Rep.* **2018**, *8* (1), 16891.

(147) Didari-Bader, A.; Pinar Mengüç, M. Near-field radiative transfer for biologically inspired structures. In *Light, Plasmonics and Particles*; Pinar Mengüç, M., Francoeur, M., Eds.; Elsevier, May 2023; Chapter 22.

(148) Choi, S. H.; Kim, S.-W.; Ku, Z.; Visbal-Onufrak, M. A.; Kim, S.-R.; Choi, K.-H.; Ko, H.; Choi, W.; Urbas, A. M.; Goo, T.-W.; Kim, Y. L. Anderson light localization in biological nanostructures of native silk. *Nat. Commun.* **2018**, *9* (1), 452.

(149) Hsu, P.-C.; Song, A. Y.; Catrysse, P. B.; Liu, C.; Peng, Y.; Xie, J.; Fan, S.; Cui, Y. Radiative human body cooling by nanoporous polyethylene textile. *Science* **2016**, *353* (6303), 1019–1023.

(150) Tong, J. K.; Huang, X.; Boriskina, S. V.; Loomis, J.; Xu, Y.; Chen, G. Infrared-transparent visible-opaque fabrics for wearable personal thermal management. *ACS Photonics* **2015**, *2* (6), 769–778.

(151) Catrysse, P. B.; Song, A. Y.; Fan, S. Photonic structure textile design for localized thermal cooling based on a fiber blending scheme. *ACS Photonics* **2016**, *3* (12), 2420–2426.

(152) Hsu, P.-C.; Liu, C.; Song, A. Y.; Zhang, Z.; Peng, Y.; Xie, J.; Liu, K.; Wu, C.-L.; Catrysse, P. B.; Cai, L.; Zhai, S.; Majumdar, A.; Fan, S.; Cui, Y. A dual-mode textile for human body radiative heating and cooling. *Science Advances* **2017**, *3* (11), No. e1700895.

(153) Peng, Y.; Chen, J.; Song, A. Y.; Catrysse, P. B.; Hsu, P.-C.; Cai, L.; Liu, B.; Zhu, Y.; Zhou, G.; Wu, D. S.; Lee, H. R.; Fan, S.; Cui, Y. Nanoporous polyethylene microfibres for large-scale radiative cooling fabric. *Nature Sustainability* **2018**, *1* (2), 105–112.

(154) Hsu, P. C.; Li, X. Photon-engineered radiative cooling textiles. *Science* **2020**, *370* (6518), 784–785.

(155) Cai, L.; Song, A. Y.; Li, W.; Hsu, P.-C.; Lin, D.; Catrysse, P. B.; Liu, Y.; Peng, Y.; Chen, J.; Wang, H.; Xu, J.; Yang, A.; Fan, S.; Cui, Y. Spectrally selective nanocomposite textile for outdoor personal cooling. *Adv. Mater.* **2018**, *30* (35), 1802152.

(156) Peng, Y.; Cui, Y. Advanced textiles for personal thermal management and energy. *Joule* **2020**, *4* (4), 724–742.

(157) Luo, H.; Li, Q.; Du, K.; Xu, Z.; Zhu, H.; Liu, D.; Cai, L.; Ghosh, P.; Qiu, M. An ultra-thin colored textile with simultaneous solar and passive heating abilities. *Nano Energy* **2019**, *65*, 103998.

(158) Luo, H.; Zhu, Y.; Xu, Z.; Hong, Y.; Ghosh, P.; Kaur, S.; Wu, M.; Yang, C.; Qiu, M.; Li, Q. Outdoor personal thermal management with simultaneous electricity generation. *Nano Lett.* **2021**, *21* (9), 3879–3886.

(159) Byers, H. R.; Landsberg, H. E.; Wexler, H.; Haurwitz, B.; Spilhaus, A. F.; Willett, H. C.; Buettner, K. J. Physical Aspects of Human Bioclimatology. In *Compendium of Meteorology*; Committee on the Compendium of Meteorology, 1951; pp 1112–1125.

(160) Palik, E. D., Ed.; *Handbook of Optical Constants of Solids*, Vol. 3; Academic Press, 1998.

(161) Siefke, T.; Kroker, S.; Pfeiffer, K.; Puffky, O.; Dietrich, K.; Franta, D.; Ohlidal, I.; Szeghalmi, A.; Kley, E.-B.; Tunnermann, A. Materials pushing the application limits of wire grid polarizers further into the deep ultraviolet spectral range. *Advanced Optical Materials* **2016**, *4* (11), 1780–1786.